Regulation of Mammalian Phosphoglycolate Phosphatase

Regulation der Phosphoglykolat-Phosphatase von Säugetieren

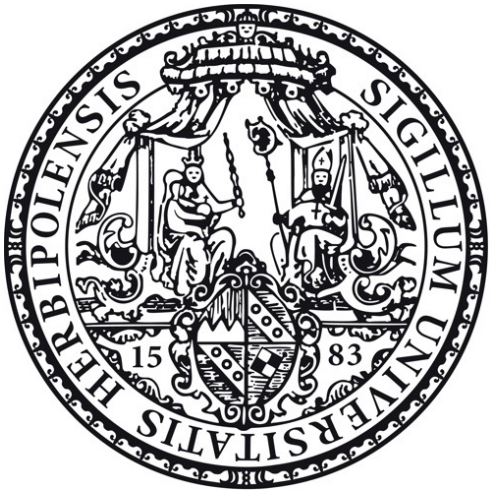

Doctoral Thesis

for a Dental Doctoral Degree
at the Graduate School of Life Sciences,
Julius-Maximilians-Universität Würzburg,
Section Biomedicine

submitted by

Daria Marie Engelmann

from Cologne

Würzburg, October 2019

Submitted on: _____

Members of the thesis committee

Chairperson:	Prof. Dr. med. Wolfgang Kastenmüller
Primary supervisor:	Prof. Dr. Antje Gohla
Supervisor (Second):	Prof. Dr. Stefan Gaubatz
Supervisor (Third):	Prof. Dr. med. Andreas Geier

Date of Public Defense: _____

Date of Receipt of Certificates: _____

The doctoral candidate is dentist.

Table of Contents

1 Introduction

1.1 Enzymatic Phospho-regulation

Phosphorylation is the esterification of phosphate $(PO_4)^{3-}$ with the hydroxyl or amino group of a molecule. This can be either an amino acid (particularly arginine, lysine, aspartate, cysteine, glutamate, histidine, serine, threonine, and tyrosine) or lipids, carbohydrates, nucleosides, and other small metabolites. (Berg et al., 2018)

If the phosphate is derived from ATP, the catalyzing enzyme is called kinase. The binding of inorganic phosphate to target molecules is performed by so called phosphorylases. Phosphatases execute the dephosphorylation as a back reaction. Protein kinases and phosphatases regulate enzyme activity as post-translational modifications for intracellular signaling, whereas metabolic kinases and phosphatases control metabolite processing important for energy production as well as anabolic and catabolic pathways. (Berg et al., 2018)

In reality, separation of the enzymatic targets and functions is not that simple: some metabolic kinases (such as pyruvate kinase) and phosphatases (such as pyridoxal phosphatase) have been identified to act on intermediary metabolites and proteins (Lu and Hunter, 2018, Gohla, 2018). Moreover, not all reactions in the organism are textbook-like and error-free. Unwanted side products can be neutralized by housekeeping enzymes including a number of phosphatases (Linster et al., 2013, Collard et al., 2016).

Phosphate esters are sufficiently charged to prevent spontaneous hydrolysis. In addition, they are thermodynamically unstable, but kinetically stable, whereby an energy release by enzymes can be controlled. Some metabolites are also phosphorylated to prevent diffusion through the cell membrane due to the attached negative charge (Berg et al., 2018). Proteins in eukaryotes are mainly phosphorylated at amino acids with a hydroxyl group - serine, threonine, and tyrosine (Olsen et al., 2006) - as well as histidine (Fuhs and Hunter, 2017). Protein phosphorylation can occur on multiple sites by different

kinases who themselves often target up to 20 substrates (Humphrey et al., 2015). Notably, 20 % of the known kinases act on nearly 90 % of the known substrates and the majority of reported phosphorylation sites could not yet be linked to a function or a responsible kinase (Needham et al., 2019). So, much of the phosphoproteome and phospho-regulation are still unknown.

Dysregulation of phosphorylation and dephosphorylation can cause severe diseases like several cancers, Alzheimer's disease and diabetes in humans (Seifried et al., 2013, Berg et al., 2018, Needham et al., 2019). For example, epithelial tumors such as breast, ovarial, or intestinal cancer are linked to hyperactivity of the receptor tyrosine kinase family of epidermal growth factor receptors (EGFR) (Berg et al., 2018). In type II diabetes regulatory serine/threonine kinases can be activated in case of supernutrition or other stressors and promote insulin resistance (Berg et al., 2018). Furthermore, some naturally occurring toxins such as okadaic acid causing diarrheic seafood poisoning inhibit certain protein serine/threonine phosphatases (Cohen, 2001).

1.2 HAD Phosphatases

Haloacid dehalogenase (HAD) hydrolases form a large and ubiquitous superfamily found in all domains of organisms, which mainly catalyze the transfer of phosphoryl residues. Most of them are phosphatases (ca. 79 %) and ATPases (ca. 20 %); phosphonatases, dehalogenases, and sugar phosphomutases play a subordinate role (Koonin and Tatusov, 1994, Allen and Dunaway-Mariano, 2009). The following is confined on the description of HAD phosphatases. In contrast to other phosphatases they consist of two domains: a core important for catalysis and a cap important for substrate specificity (Seifried et al., 2013).

1.2.1 Core Domain and Catalytic Mechanism

Although the overall structure may differ within the family (amino acid sequence identity often < 15 %), all HAD phosphatases share the Rossmannoid fold in their catalytic core. Its three-layered α/β- sandwich consists of repeating β-α units, the central parallel

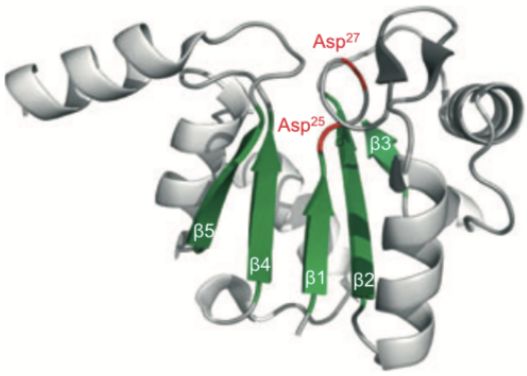

Figure 1. The Rossmannoid fold of the catalytic core of PDXP.
(adapted PDB: 2P69, modified) HAD phosphatases share the repeating ß-α units. Highlighted are the five sequentially arranged ß-strands of the central sheet (green), the two aspartates of HAD motif I (red), and the squiggle and flap domains in (dark gray). The figure is adapted from (Seifried et al., 2013). John Wiley and Sons license: 4691260436173.

β-sheet is typically comprised of at least five strands in a '54123' sequence. Along these four conserved HAD signature motifs are essential for catalysis. The typical “squiggle” - a nearly complete single helical turn - is located downstream of the first strand and it is followed by a conserved ß-hairpin named “flap”. Motif I (the first strand) with the consensus sequence hhhDXDX(T/V)(L/V)h includes the nucleophilic aspartate (Asp25 in PDXP, figure 1), whose carboxylate group also coordinates the necessary Mg^{2+} together with the carbonyl group of the second aspartate. The serine or threonine of the consensus sequence hhhhhh(S/T) of motif II coordinates the substrate towards the nucleophilic attack and stabilizes the phosphoaspartyl intermediate in cooperation with the central lysine of motif III. The aspartate or glutamate residues of motif IV with the common consensus sequence (G/S)(D/S)x_{3-4}(D/E)hhhh help orienting the cofactor Mg^{2+}. (Seifried et al., 2013, Burroughs et al., 2006)

For the dephosphorylation, first, the nucleophilic aspartate attacks the phosphoryl group of the substrate forming a phosphoaspartyl enzyme intermediate and dissociating the substrate leaving group. Second, a water molecule effects another nucleophilic attack releasing free phosphate and regenerating the catalytic aspartate. A second aspartate (Asp+2, positioned two residues behind the nucleophile; Asp27 in PDXP, figure 1) protonates the leaving group in the first part and deprotonates the H_2O nucleophile in the second part of the reaction. The dicationic metal ion Mg^{2+} enables the approach of the anionic nucleophile to the dianionic substrate phosphomonoester by electrostatic stabilization and connects the substrate phosphoryl group and the nucleophilic aspartate. (Allen and Dunaway-Mariano, 2009)

1.2.2 Cap Domain and Substrate Specificity

Most HAD phosphatases additionally possess cap domains guaranteeing substrate specificity, because the size of the target molecules is very diverse. These cap modules can be divided into three categories depending on location and topology of the insert: C0, C1 and C2. C0 and C1 caps share the insert site but can be distinguished by length and complexity of the insert. C2 caps as the most "sophisticated" ones can be further divided in the two subgroups C2a and C2b. The cap structures allow conformational changes ("open"/"close" dynamics especially in the case of C1 caps) to modulate solvent entry or exclusion at the active site. Enzymes with a small C0 cap target macromolecular substrates more easily. The larger C1 and C2 caps limit the access to the catalytic core, so that these enzymes preferentially convert substrates of low molecular weight. (Burroughs et al., 2006, Allen and Dunaway-Mariano, 2009)

Until now, only two phosphatases capped in such a way have been identified to act on macromolecules: C1-capped Eya3 dephosphorylates the C-terminal tyrosyl residue of histone H2A.X (Krishnan et al., 2009) and C2-capped pyridoxal phosphatase (PDXP; also called chronophin, CIN) dephosphorylates pyridoxal 5'-phosphate (PLP, the active form of vitamin B6) (Jang et al., 2003, Kestler et al., 2014, Jeanclos et al., 2019) as well as a serine residue of the actin-binding protein cofilin (Gohla et al., 2005).

A couple of HAD phosphatases have been linked to cancer, cardiovascular, metabolic, or neuropsychiatric diseases (Seifried et al., 2013). For example, PDXP is involved in glioblastoma (Schulze et al., 2016); phospholysine phosphohistidine inorganic pyrophosphate phosphatase (LHPP) was suggested as a biomarker for major depression (Neff et al., 2009) and as tumor suppressor in hepatocellular carcinoma (Hindupur et al., 2018). Hence, targeting these enzymes with pharmacological tools is of great interest both in terms of fundamental and applied research questions.

1.3 Phosphoglycolate Phosphatase

Mammalian phosphoglycolate phosphatase (PGP) is a broadly expressed cytosolic enzyme of the HAD-type superfamily (Seifried et al., 2013). The enzyme is also known as

AUM, meaning aspartate-based, ubiquitous, Mg^{2+}-dependent phosphatase, glycerol-3-phosphate phosphatase, 2-phospho-L-lactate phosphatase, and 4-phosphoerythronate phosphatase (Seifried et al., 2014, Mugabo et al., 2016, Collard et al., 2016).

PGP is ubiquitously expressed in mammalian tissues, although the highest levels are found in testis followed by skeletal muscle and heart (Seifried et al., 2014, Mugabo et al., 2016). Like all phosphoryltransferases of the HAD superfamily, PGP depends on the abundance of the divalent metal ion Mg^{2+}, which helps orienting the substrate in the catalytic core (compare 1.2.1). Chelating Mg^{2+} by EDTA (5 mM) or displacing Mg^{2+} by Ca^{2+} (IC_{50} = 0.5 mM) inhibit the phosphatase (Seifried et al., 2014).

1.3.1 Protein Structure

PGP can be classified as a member of the C2-capped NagD-like phosphatases subfamily (Burroughs et al., 2006), more precisely of the C2a-type that predetermines for the hydrolysis of low molecular weight substrates (Seifried et al., 2014).

A crystallographic analysis of full-length PGP has not been successful yet. However, it was possible to crystallize a PDXP(1–100)-PGP(114-233)-PDXP(208–292) hybrid (consisting of the PGP cap and the PDXP core domain, from now on referred to as

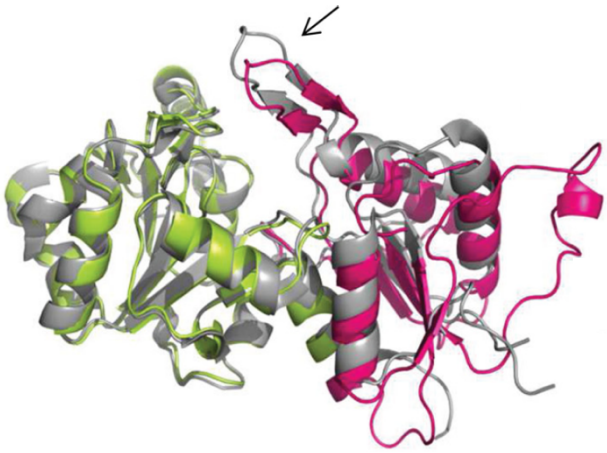

Figure 2. Crystal structure of the murine PGP/PDXP hybrid.
Overall structure of the PDXP core/PGP cap hybrid (PDB 4BKM) compared with human PDXP in the pyridoxal 5'-phosphate-bound state (PDB 2P69). PDXP (gray); hybrid: murine PDXP core (lime), PGP cap (pink). The catalytic cores of human and murine PDXP are organized in a superimposable manner, whereas the PGP and PDXP caps differ. PGP substrate specificity loop (arrow). This research was originally published in the Journal of Biological Chemistry. Seifried A., Knobloch G., Duraphe P. S., Segerer G., Manhard J., Schindelin H., Schultz J. and Gohla A. Evolutionary and Structural Analyses of Mammalian Haloacid Dehalogenase-type Phosphatases AUM and Chronophin Provide Insight into the Basis of Their Different Substrate Specificities. J. Biol. Chem. 2014; 289:3416-3431. © the American Society for Biochemistry and Molecular Biology or © the Authors.

PGP/PDXP hybrid; figure 2) from murine proteins (Seifried et al., 2014). In the HAD superfamily PDXP is the closest paralog of PGP: the overall amino acid sequence matches by 45 % between the murine enzymes and by 47 % between the human ones. The core domain residues involved in catalysis of these two phosphatases are nearly identical (except for Thr-67 in PGP that orientates the substrate for the nucleophilic attack). The cap domain containing the so-called substrate specificity loop (a ß-hairpin covering the entrance to the active site) shows differences. Leu-204 in PGP/Leu-191 in the PGP/PDXP hybrid corresponding to His-182 in PDXP were identified as critical residues within the substrate specificity loop. It thus appears comprehensible that the PGP/PDXP hybrid does not remarkably dephosphorylate the PDXP substrate PLP. A PGP(1-113)-PDXP(101-207)-PGP(234-321) hybrid (consisting of the PDXP cap and the PDXP core domain) was indeed active towards PLP. (Seifried et al., 2014)

1.3.2 Dephosphorylation of Potentially Toxic Metabolites

PGP specifically dephosphorylates small metabolites that may be generated during oxidative DNA damage repair and glycolysis, namely 2-phosphoglycolate (PG), 2-

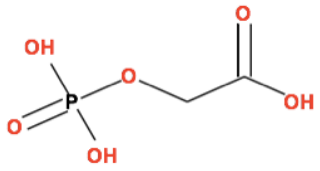

2-phosphoglycolate

Mol. weight	156.03 g/mol
K_M	139 µM
k_{cat}	22.6 ± 0.6 s^{-1}

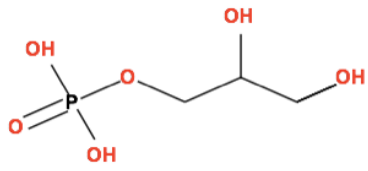

Sn-glycerol 3-phosphate

Mol. weight	172.07 g/mol
K_M	1.29 ± 0.42 mM
k_{cat}	0.10 ± 0.01 s^{-1}

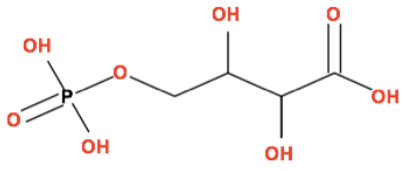

4-phospho-D-erythronate

Mol. weight	216.08 g/mol
K_M	247 ± 25 µM
k_{cat}	3.23 ± 0.18 s^{-1}

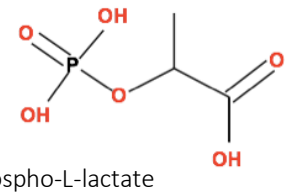

2-phospho-L-lactate

Mol. weight	168.04 g/mol
K_M	174 ± 55 µM
k_{cat}	1.82 ± 0.34 s^{-1}

Figure 3. Chemical structures of the physiological substrates of PGP.
Data (structure and molecular weight) from National Center for Biotechnology Information, PubChem Compound Database. All K_M and k_{cat} values represent the activity of purified murine PGP. The K_M and k_{cat} values for PG-dephosphorylation were determined within this work as an average of all experiments (figures 16A and 18, tables 11 and 13), the others are taken from (Collard et al., 2016) for 2PL and 4PE as well as (Seifried et al., 2016) for Gro3P.

phospho-L-lactate (2PL), 4-phospho-D-erythronate (4PE), and glycerol 3-phosphate (Gro3P) (figures 3 and 4) (Seifried et al., 2016, Mugabo et al., 2016, Collard et al., 2016). As three of the mentioned substrates are potent inhibitors of important metabolic enzymes *in vitro*, PGP's key task might be housekeeping (Collard et al., 2016).

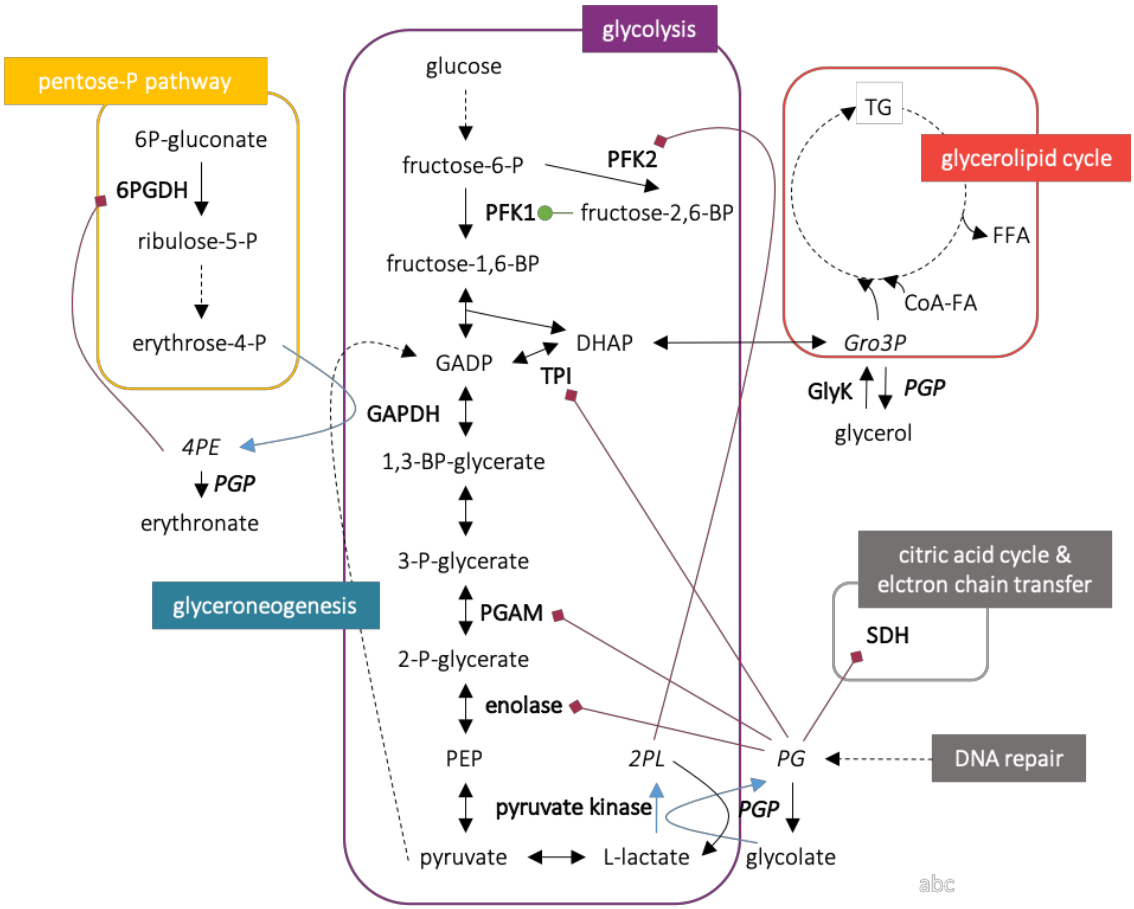

Figure 4. Rough overview of PGP's substrates and their role in important metabolic pathways.
(6PGDH = 6-phosphogluconate dehydrogenase, BP = bisphospho- or bisphosphate, CoA-FA = fatty acids activated by coenzyme A, DHAP = dihydroxyacetone phosphate, FFA = free fatty acids, GADP = glyceraldehyde-3-phosphate, GAPDH = glyceraldehyde 3-phosphate dehydrogenase, GlyK= glycerokinase, P = phospho- or phosphate, PEP = phosphoenolpyruvate, PFK = phosphofructokinase, PGAM = phosphoglycerate mutase, SDH = succinate dehydrogenase, TPI = triosephosphate isomerase) Enzymes are emboldened, PGP and its potential substrates are italicized; black arrows mark catalyzed reactions, dashed black arrows skip one or several reactions, light blue arrows mark "unwanted" side reactions, dark red arrows with a square end mark inhibitory effects, the light green arrow with a circle end marks activation. The depiction of the metabolic pathways raises no claim to completeness. It is confined on the most basal metabolites, enzymes, and reactions that are important to better understand the role of PGP. The figure is inspired by (Collard et al., 2016) and completed.

1.3.2.1 2-Phosphoglycolate (PG)

PG can be produced by the phosphorylation of glycolate (figure 5A). Pyruvate kinase is reported to show a glycolate kinase activity in yeast, rabbit muscle, red blood

cells, and human colorectal carcinoma cells (HCT116) (Leblond and Robinson, 1976, Kayne, 1974, Fujii and Beutler, 1985, Gerin et al., 2019). The amount of PG synthesis by pyruvate kinase does not seem to account for physiological PG levels in red blood cells (Fujii and Beutler, 1985). However, in HCT116 cells phosphorylation of glycolate by pyruvate kinase seems to be a major source of PG after exogenous addition of 5 mM glycolate (Gerin et al., 2019). Glycerate kinase also phosphorylates glycolate, albeit to a rather limited extent in HCT116 cells (Gerin et al., 2019). PG can also be derived from the repair of oxidative DNA damage (figure 5B). DNA strand breaks are most commonly caused by reactive oxygen species (ROS). The cell provides several repair mechanisms. When certain single or double strand breaks show a 3'-PG end, phosphodiesterases such as apurinic/apyrimidinic endonuclease 1 (APE1) (Fung and Demple, 2011, Iyama and Wilson, 2013) or Aprataxin (Takahashi et al., 2007) can generate appropriate 3'-OH ends for further DNA repair by cleaving off and releasing PG. Still, there might be other yet unknown reactions. Since both PG and PGP levels differ intracellularly in different tissues, PG formation could be differentially weighted. *In vitro*, PGP is an efficient and to date the only reported PG phosphatase which makes cytosolic PG a candidate substrate for PGP in cells (figure 3, $K_M \approx 139$ µM) (Seifried et al., 2016, Segerer et al., 2016, Gerin et al., 2019).

PG is reported to inhibit several enzymes involved in important metabolic pathways. It blocks the triose phosphate isomerase (TPI, $K_i \approx 4\text{-}15$ µM), a key glycolytic enzyme operating at the intersection between glucose and lipid metabolism (Anderson, 1971). TPI activity was reduced up to 34 % in PGP inactivated erythrocytes and embryo explants (Segerer et al., 2016). PG can further inhibit enolase ($K_i \approx 160$ µM) (Gerin et al.,

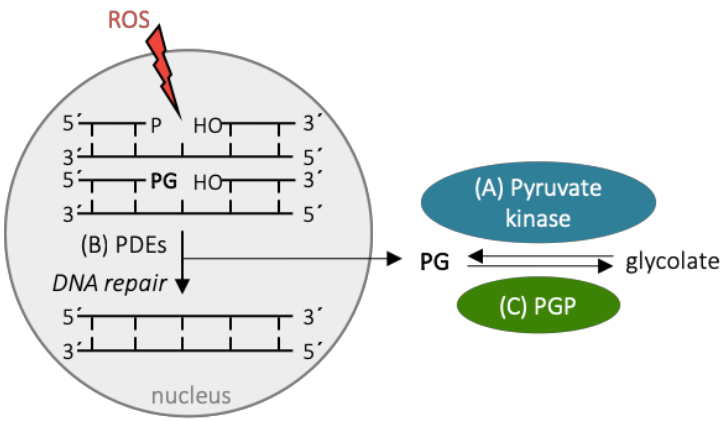

Figure 5. PG formation and degradation.
(A) Pyruvate kinase can directly phosphorylate glycolate. (B) Single strand DNA breaks induced by ROS (reactive oxygen species) lead to the formation of 3'-PG ends. PDEs (phosphodiesterases) can cleave off PG and release it into the cytosol to enable further DNA repair. (C) PGP can dephosphorylate PG. The figure is adapted from (Segerer, 2015).

2019). PG can affect phosphoglycerate mutase (PGAM) that has three different activities: as mutase for the interconversion of 2-phosphoglycerate and 3-phosphoglycerate, as phosphatase of 1,2- or 1,3-bisphosphoglycerate (BPG) and as BPG synthase (Rose and Dube, 1978). PG indirectly inhibited the mutase activity of PGAM (Gerin et al., 2019) and promoted the activity as 2,3-BPG phosphatase (K_a ≈ 30-120 µM) (Rose and Liebowitz, 1970). PGAM's phosphatase activity was inhibited in the simultaneous presence of PG and glycolate (Rose and Liebowitz, 1970) and by PG at too low 2,3-BPG concentrations (Rose and Dube, 1978). PG is also a competitive inhibitor of succinate dehydrogenase (K_i < 10 µM) which operates in citric acid cycle and electron transport chain in mitochondria (Gerin et al., 2019) and phosphoenolpyruvate carboxykinase (K_i ≈ 1 mM), which plays a role in gluconeogenesis (Stiffin et al., 2008). However, PG levels in mammalian cells appear to be quite low (< 5 to 20 µM in HCT116 colorectal cancer cells, U2OS osteosarcoma cells, or liver tissue) and do not drastically increase in PGP-deficient cells to levels relevant for inhibition of the forenamed enzymes (Gerin et al., 2019, Mugabo et al., 2016). Therefore, the physiological importance of PG-dephosphorylation in mammals remains unclear.

1.3.2.2 2-Phospho-L-Lactate (2PL)

Another side product of pyruvate kinase, and a substrate of PGP is 2PL (K_M ≈ 174 µM) (Collard et al., 2016). So far, its sole reported function is the inhibition of phosphofructokinase 2 (depending on the isozyme in different cell types) the product of which activates phosphofructokinase 1 upstream of pyruvate kinase in glycolysis. 2PL levels are in fact elevated in PGP-deficient cells (up to 2-4 mM) and a pre-emptive dephosphorylation by PGP might prevent a blockade of glycolysis. (Gerin et al., 2019, Collard et al., 2016)

1.3.2.3 4-Phospho-D-Erythronate (4PE)

Glyceraldehyde 3-phosphate dehydrogenase, also of major importance during glycolysis, can accidently form 4PE. PGP can also dephosphorylate 4PE (K_M ≈ 247 µM) although a little less effectively than PG and 2PL (Collard et al., 2016). 4PE concentrations

in PGP deficient cells were at least 10-fold increased (up to 20-30 µM) and caused an inhibition of the pentosephosphate pathway enzyme 6-phosphogluconate dehydrogenase (IC_{50} < 1 µM for humans and yeast; note that the sheep liver enzyme is remarkably less sensitive to inhibition) and accumulation of 6-phosphogluconate (Collard et al., 2016). Nevertheless, an alteration of the NADPH/$NADP^+$ ratio that would be expected from an impaired pentose phosphate pathway activity could not be observed (Collard et al., 2016). Yet, different (and pentose phosphate pathway independent) pathways for NADPH production might exist in different cell types, and indeed there were controversial reports of PGP-related changes in NADPH/$NADP^+$ ratio (Segerer et al., 2018, Mugabo et al., 2016).

1.3.2.4 Glycerol-3-Phosphate (Gro3P)

Another substrate of PGP is Gro3P which is required in the glycerolipid/free fatty acid cycle as activated backbone of triacylglycerides (TG) (Berg et al., 2018). Gro3P can be derived from glycolysis, glyceroneogenesis, and phosphorylation of glycerol by glycerokinase (Prentki and Madiraju, 2008). Glucose metabolism leads to the formation

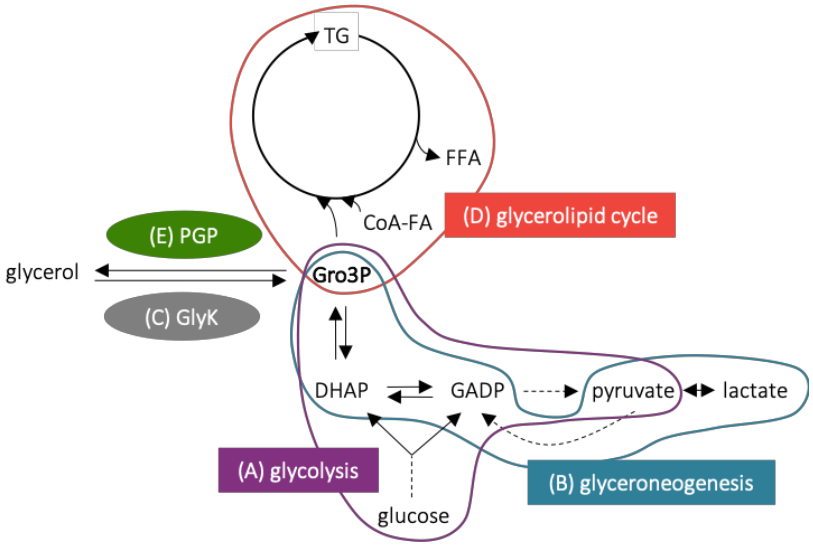

Figure 6. Gro3P formation and use.
(A) Glucose metabolism leads to the formation of the triosephosphates GADP (glyceraldehyde-3-phosphate) and DHAP (dihydroxyacetone phosphate). Whilst GADP is further processed to pyruvate to generate energy, DHAP can be reduced to Gro3P (glycerol-3-phosphate). (B) Glycerogenesis means a de novo-synthesis of glycerol from other metabolites than glucose, presumably pyruvate, lactate, and amino acids. (C) Also, glycerol can be directly phosphorylated by GlyK (glycerokinase). (D) Gro3P can enter the glycerolipid cycle as backbone for TG (triacylglyceride) buildup. For lipogenesis three fatty acids activated by coenzyme A (CoA-FA) are consecutively esterified to Gro3P; for lipolysis free fatty acids (FFA) are hydrolysed and released.

of the triosephosphates glyceraldehyde-3-phosphate (GADP) and dihydroxyacetone phosphate (DHAP). Whilst GADP is further processed to pyruvate to gain energy, DHAP can be reduced to Gro3P. Gro3P can then enter the glycerolipid cycle (Berg et al., 2018). Glycerogenesis means a de novo-synthesis of glycerol from other metabolites than glucose, presumably pyruvate, lactate, and amino acids (Nye et al., 2008). It thus stands at the intersection between glucose and lipid metabolism. PGP is capable to dephosphorylate Gro3P ($K_M \approx 1.29$ mM), although considerably less effectively than PG. But for housekeeping the enzyme might work effectively enough, because physiological levels of Gro3P (2.0-4.5 mM in primary rat hepatocytes) are up to 250-fold higher than PG levels (Mugabo et al., 2016). Figure 6 shows an overview of Gro3P metabolism.

In embryos with a whole-body knock-in of phosphatase-inactivated PGP^{D34N} replacing PGP^{WT}, Gro3P levels were about 50 % elevated, supposedly being the result of TPI inhibition favoring DHAP-, and in consequence Gro3P formation, and/or reduced dephosphorylation of Gro3P by PGP (Segerer et al., 2016). The Gro3P content was up to 49 % higher in PGP downregulated cells (via siRNA or shRNA) compared to control cells upon glucose addition (mimicking metabolic overload) favoring DHAP formation via glycolysis (Segerer et al., 2018, Mugabo et al., 2016). Otherwise Gro3P levels do not seem to change upon PGP knockout in tumor cells (Gerin et al., 2019).

1.3.3 Role of PGP in Biological Processes

PGP activity and its control seem to contribute to a balanced cellular lipid metabolism and proliferation of cells.

1.3.3.1 Glycerolipid Partitioning and Proliferation

Next to higher Gro3P levels an altered lipid metabolism was observed (Segerer et al., 2016, Segerer et al., 2018). Around 25 % elevated triacylglyceride (TG) levels and 40 % reduced phosphatidylcholine content (essential component of the cellular membrane) might account for lipid droplet accumulation and reduced proliferation of the observed murine embryonic fibroblasts in the two studies of Segerer et al. These mechanisms seem to be of a high importance in embryonic development since a whole-

body knockin replacement of PGP by a phosphatase-inactive enzyme mutant resulted in a retardation in development from embryonic day (E) 8.5 on (the starting point of maternal/fetal gaseous exchange) and embryonic lethality (Segerer et al., 2016). Hypoxia (ca. 1% O_2; normoxia in cell culture ≈ 20 % O_2) normalized TG and phosphatidylcholine content as well as proliferation in murine embryonic fibroblasts derived from E8.5 embryo explant cultures (Segerer et al., 2016). For the examined murine embryonic fibroblasts 3 % of O_2 would be physiological (Parrinello et al., 2003). The proliferation defect or growth retardation were supposedly effects of increased oxidative stress in organisms lacking PGP activity (Segerer et al., 2016, Segerer et al., 2018).

In vivo overexpression of PGP in rat livers in contrast reduced plasma TG levels and body weight gain (Mugabo et al., 2016). The impact of PGP overexpression on proliferation has not been investigated yet. Lipid metabolism and embryo growth and development seem to be connected with PGP activity, but by far not all of the forenamed effects can currently be explained by a primary effect on Gro3P levels.

1.3.3.2 Epidermal Growth Factor Signaling

PGP shRNA cells show enhanced circular dorsal ruffle formation after stimulation with epidermal growth factor (EGF) (Segerer et al., 2018). Circular dorsal ruffles (CDRs) are transient ring-shaped apical membrane protrusions important for the incorporation of growth-factor receptors and migration (Hoon et al., 2012). This kind of cytoskeletal remodeling in PGP shRNA cells could be linked to increased formation of phosphatidylinositol 4,5-bisphosphate (PIP_2, as result of altered glycerolipid cycling) as well as hyperphosphorylation of EGF receptor (EGFR) after its stimulation (Segerer et al., 2018). PGP downregulation is already known to elevate levels of tyrosyl-phosphorylated proteins upon EGFR stimulation (Seifried et al., 2014). Although PGP was able to hydrolyze denatured tyrosyl-phosphorylated proteins from human cervical cancer cells *in vitro* a physiological protein substrate could not be identified yet (Seifried et al., 2014).

1.3.4 Physiological and Experimental PGP Activity Control

Physiological as well as experimental control mechanisms of enzymatic activity can provide new insights into the enzyme's mode of action and role in cellular physiology.

1.3.4.1 Reversible Thiol Oxidation

Protein thiol oxidation is an important regulatory mechanism in the context of cell surface receptor related signaling (Rhee et al., 2000). Ligand-binding peptide growth factor receptors such as EGFR induces ROS production e.g. by NADPH oxidases (Heppner and van der Vliet, 2016). ROS such as superoxide anions, hydroxyl radicals, or H_2O_2 can oxidize enzymes on cysteine, methionine, proline, histidine, and tryptophan residues, a reaction with decreasing likelihood of reversal by low molecular weight and protein thiols in the order mentioned. The reversibility of cysteine-based redox switches (as predominant regulating system) depends on the oxidation state (sulfenic, sulfinic, or sulfonic) (Sies et al., 2017). Higher oxidation states (sulfinic acids, sulfinamides, sulfonic acids, sulfonamides, etc.) cannot be easily reversed by reduction systems like glutathione but are irreversible in most cases or require special ATP-consuming processes (Klomsiri et al., 2011). A transient and reversible oxidation can modulate enzyme activity e.g. activate kinases downstream of EGFR and/or inhibit protein tyrosine phosphatases (PTPs) as their antagonists (Rhee et al., 2000). Some of these proteins can be directly inhibited by oxidation of their catalytic cysteine residue (especially PTPs), others contain regulatory cysteine residues apart from the active site (Klomsiri et al., 2011).

PGP was identified as the first enzyme of the HAD phosphatase family whose activity can be modulated by reversible oxidation (figure 7) (Seifried et al., 2016). This is interesting because the catalytic mechanism of HAD phosphatases is not based on cysteine like PTPs (and thus directly sensitive to oxidation) but on aspartate that cannot be oxidized. The activity of the HAD phosphatases phospholysine phosphohistidine inorganic pyrophosphate phosphatase (LHPP) and magnesium dependent phosphatase 1 (MDP1) was not redox dependent (Frankenbach, 2017). Seifried et al. revealed that PGP's

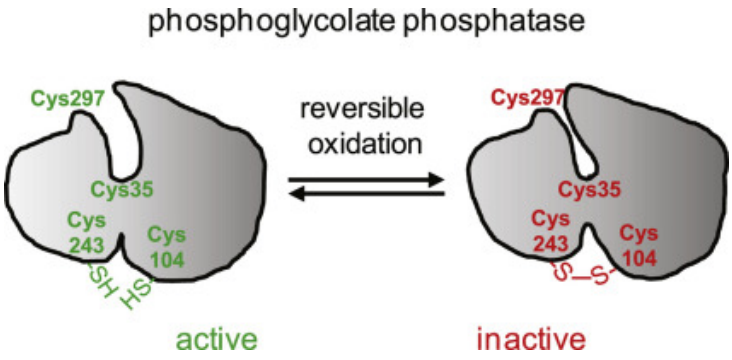

Figure 7. PGP inactivation by oxidation of conserved cysteine residues.
Schematic depiction. The figure is adapted from (Seifried et al., 2016). Elsevier license: 4691260775639.

oxidative inactivation is associated with three conserved cysteine residues that are not directly involved in catalysis. Cys35 located in the active cleft is supposed to influence the positioning of Thr67 (that orientates the substrate for the nucleophilic attack, see 1.2.1). Replacing the thiol moiety of Cys35 with an alcohol or its oxidation by exogenous H_2O_2 inhibits the activity of purified PGP *in vitro*. Cys104 and Cys243 located at the interface of the core/cap domain interaction might influence PGP's open/close dynamics. Oxidation enables a disulfide bond formation between Cys104 and Cys243. Exchanging them (both or individually) to serine residues makes PGP less sensitive to inhibition by H_2O_2. (Seifried et al., 2016)

In addition, a further cysteine residue was identified, the oxidation of which favored PGP oligomerization (of note, oligomerization does not affect PGPs catalytical activity). Western blot analysis revealed an increase in PGP oligomers in cells treated with H_2O_2 or EGF (as inducer of physiological ROS production after receptor stimulation). The amount of PGP oligomers showed a peak 2 minutes after H_2O_2 treatment followed by regression. This suggests that H_2O_2 or activation of the EGF signaling pathway can also reversibly inhibit PGP activity intracellularly. (Seifried et al., 2016)

1.3.4.2 Phosphatase Inhibitors

Phosphatase inhibitors can be used as broad-spectrum inhibitors for studying phosphosignaling or the phosphoproteome (Dewang et al., 2005, Swingle et al., 2007, Fontanillo and Kohn, 2016). In this case, they are usually competitive inhibitors that target many phosphatases within a family (most of all PTPs and PSTPs) with the same catalytic

mechanism (and structurally similar catalytic subunits). PTPs and PSTPs are the biggest and best studied phosphatase families so far - each with a highly conserved active site. However, despite structurally and mechanistically similar catalytic subunits, PTPs or PSTPs can have very different physiological functions (due to differing substrate specificity, including various combinations of additional regulatory subunits for PSTPs). It is therefore usually not possible to specifically influence individual enzyme reactions with competitive PTP or PSTP inhibitors (Dewang et al., 2005, Swingle et al., 2007). As PTPs and PSTPs are increasingly brought into focus in cancer research, a number of selective inhibitors have been identified in recent decades, which are more likely to bind allosterically to specific subunits of the targeted enzymes (Fontanillo and Kohn, 2016).

In contrast, specific HAD phosphatase inhibitors are largely lacking. The aspartate-based catalytic mechanism and the cap domains responsible for substrate specificity distinguish HAD phosphatases from PTPs and PSTPs. Similar to other HAD phosphatases, PGP can be inactivated by BeF_3^- that is normally used as a tetragonal ground state analogue of phosphate and phosphoaspartyl mimic for structural analyses of phosphatases (Seifried et al., 2014, Cho et al., 2001). Within the family of HAD phosphatases, PGP was discussed as protein tyrosine phosphatase although the catalytic mechanism differs from that of the family of PTPs (Seifried et al., 2014). The planar phosphate mimic and transition state analogue orthovanadate used as PTP inhibitor could block PGP activity (IC_{50} = 41.4 µM). Okadaic acid and calyculin A used as type 1 and 2A PSTP inhibitors could not inhibit PGP (Seifried et al., 2014). Some typical (phosphatase) inhibitors tested against PGP from tobacco did not show an inhibiting effect, whereas cysteine (known as inhibitor of alkaline phosphatase by chelating cofactor Zn^{2+}) could inhibit PGP from tobacco (Richardson and Tolbert, 1961, Agus et al., 1966).

1.4 Enzyme Inhibition

Enzymes are proteins involved in numerous metabolic reactions as biocatalysts by destabilizing the ground state (of its substrate) and reducing transition state energies and energetic intermediates. The inhibition or inactivation of enzymes (by drugs) is of major

interest when it comes to metabolic disorders associated with abnormal enzymatic activity. (Silverman and Holladay, 2014)

1.4.1 Enzyme Kinetics

Specificity and rate acceleration are the main characteristics of enzyme catalysis. A generalized enzyme-catalyzed reaction is schematically depicted in figure 8A. The kinetic properties of enzymes can be described and compared by the following constants. v_{max} is the maximum velocity of the reaction, where all enzymes are bound to an enzyme-substrate-complex. The Michaelis-Menten-constant (K_M) indicates the substrate ([S]) concentration, where half of all enzymes ([E]) are bound in an enzyme-substrate-complex ([ES]), respectively when half of the maximum velocity is reached. (Sharma, 2012, Berg et al., 2018)

$$K_M = \frac{[E][S]}{[ES]}$$

The catalytic constant or turnover number (k_{cat}) describes the velocity of the product building. It is the rate constant for the conversion of ES to EP (= enzyme-product-complex). (Silverman and Holladay, 2014)

The quotient of k_{cat}/K_M can be used to describe the catalytic efficiency of an enzyme (Berg et al., 2018).

1.4.2 Reaction Conditions

In general, most enzymes are dependent on the availability of one or several obligatory co-factors, which are mostly metal ions. As described above mammalian PGP requires Mg^{2+} (Seifried et al., 2014). PGP from Tobacco for example is activated upon addition of Co^{2+} or Zn^{2+} (Richardson and Tolbert, 1961). The pH value plays a role: the pH optimum of PGP from *E. coli* and tobacco range around pH 6.9 or pH 6.0 - 6.3, respectively (Richardson and Tolbert, 1961, Pellicer et al., 2003). Murine PGP has a pH optimum at pH 7.5 (Seifried, 2014). The temperature can influence enzymatic activity, which is commonly slowed down at lower temperatures and enhanced at higher temperatures

with an optimum around body temperature (37°C) for mammalian enzymes (Sharma, 2012). Most proteins can be completely inactivated by heat exposure (Berg et al., 2018).

1.4.3 Mechanisms of Enzyme Inhibition

Enzyme activity can be blocked or slowed down either by occupation of the active center (competitive inhibition) or by inducing a change of the conformation and/or the chemical charge, so that the affinity towards the substrate is enhanced or reduced. The binding of molecular inhibitors to the protein can be irreversible or reversible. (Sharma, 2012, Berg et al., 2018)

Irreversible inhibition (or inactivation) occurs when a molecule binds covalently or noncovalently to the active site or destroys a crucial functional group therein. The inhibitor hardly dissociates from the enzyme; thus, the concentration of active catalysts is effectively reduced. (Sharma, 2012, Berg et al., 2018)

Upon reversible inhibition the enzyme-inhibitor-complex dissociates quite quickly. It can be further divided into competitive, uncompetitive, noncompetitive, or mixed inhibition. (Sharma, 2012, Berg et al., 2018)

A competitive inhibitor resembles the substrate structurally and competes with the substrate for the binding at the active site of the enzyme and reduces the availability of free enzyme for substrate conversion. Increasing inhibitor concentrations demand increasing substrate concentrations, so the Michaelis-Menten-constant K_M increases proportionately to the inhibitor concentration. Turnover number, catalytic efficiency, and v_{max} do not change as free enzymes act normally (figure 8B). An elevated substrate concentration can reverse the inhibitory effect. Also and in general, enzymes are reversibly and competitively inhibited by their products. (Sharma, 2012, Berg et al., 2018)

The dissociation constant (K_i) describes the concentration where free enzyme and free inhibitor are in equilibrium with enzyme bound by inhibitor (Sharma, 2012, Berg et al., 2018):

$$K_i = \frac{[E][I]}{[EI]}$$

Its influence on the changed "apparent" K_M upon addition of a competitive inhibitor can be depicted as follows (Sharma, 2012, Berg et al., 2018):

$$K_M^{app} = K_M(1+[I]/K_i)$$

Easier to determine is the half maximal inhibitory concentration (IC_{50}) that indicates when enzymatic activity is reduced to 50 %. Under steady-state conditions the K_i can be approximated by the equation below (Cheng and Prusoff, 1973, Silverman and Holladay, 2014):

$$IC_{50} = (1+[S]/K_M)K_i$$

The lower the K_i or IC_{50} the more effective is the inhibition (Silverman and Holladay, 2014).

An uncompetitive inhibitor does not resemble the substrate. Only the enzyme-substrate-(ES)-complex exposes the binding site for such an inhibitor that can form an enzyme-substrate-inhibitor-(ESI)-complex. The reduction of ES-complexes because of the formation of ESI-complexes make v_{max} decrease. This reduced ES-complex content

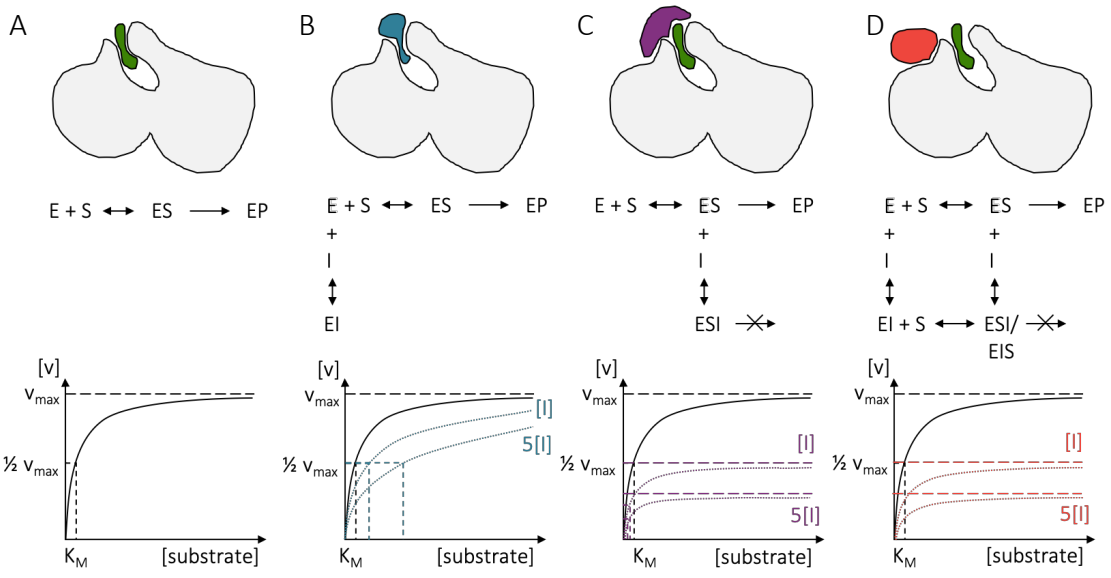

Figure 8. Schematic depiction of enzyme kinetics and the effect of different reversible inhibition mechanisms.

(A) Enzyme (E, grey) and substrate (S, green). (B) Enzyme and competitive inhibitor (I, blue). Enzyme kinetics change (dotted blue curves) relative the inhibitor concentration ([I] or 5[I] expressing a 5-fold increased concentration) causing no change in v_{max} and a progressive increase K_M (dashed blue lines). (C) Enzyme, substrate and uncompetitive inhibitor (I, violet). Enzyme kinetics change (dotted purple curves) relative to [I] causing a progressive decrease in v_{max} (dashed purple lines) and a progressive decrease in K_M (dashed purple lines). (D) Enzyme, substrate and noncompetitive inhibitor (I, red). Enzyme kinetics change (dotted red curves) relative [I] causing a progressive decrease in v_{max} (dashed red lines) and no change in K_M. The figure is inspired by (Sharma, 2012, Berg et al., 2018).

requires also less substrate and reduces the apparent K_M (figure 8C). The inhibition cannot be reversed by substrate addition. (Sharma, 2012, Berg et al., 2018)

A noncompetitive inhibitor also does not resemble the substrate. It binds allosterically either to the enzyme alone or to the ES-complex and alters its catalytic activity by a conformational change. ESI-complex formation reduces the number of ES-complexes, so that v_{max} diminishes proportionately to the inhibitor concentration. When the ESI-complex is catalytically inactive, K_M does not change. Addition of substrate cannot rescue enzymatic activity (figure 8D). (Sharma, 2012, Berg et al., 2018)

For the change of v_{max} upon real noncompetitive inhibition applies (Sharma, 2012, Berg et al., 2018):

$$v_{max}^{app} = \frac{v_{max}}{1+[I]/K_i}$$

For uncompetitive and noncompetitive inhibition K_i equals the IC_{50} value when the affinity of the inhibitor to the enzyme and the enzyme-substrate-complex is similar (Cheng and Prusoff, 1973).

A mixed inhibitor binds similar to a noncompetitive inhibitor albeit the EIS-complex has residual enzymatic activity. Still, v_{max} decreases relative to the inhibitor concentrations, but K_M increases in the fashion of competitive inhibition. (Sharma, 2012, Berg et al., 2018)

1.5 Aim of the Study

PGP is a haloacid (HAD)-type phosphatase, whose cellular and physiological functions are only beginning to emerge. Currently known PGP substrates are 2-phosphoglycolate, 2-phospho-L-lactate, and 4-phospho-D-erythronate, suggesting that PGP acts as a “housekeeping” enzyme that is required for proper glycolytic flux and in the pentose phosphate pathway. In addition, PGP dephosphorylates glycerol-3-phosphate, indicating a role at the interface between glucose and glycerolipid metabolism. Cellular studies have revealed PGP-functions in EGF signaling, and the analysis of PGP-inactivated mice has demonstrated that PGP is essential for cellular proliferation and embryonic development. These effects might be linked to its phosphoglycolate-dephosphorylating

activity in the context of oxidative DNA damage. Finally, biochemical studies have shown that PGP itself is regulated by reversible oxidation.

The aim of this thesis is

(1) to investigate the influence of reactive oxygen species (ROS) on cellular PGP activity and on PGP-dependent cell proliferation, and

(2) to biochemically characterize four small molecule PGP inhibitor candidates.

It is expected that these analyses will help to elucidate the physiological importance of reversible oxidation for PGP activity in the context of cell proliferation and pave the way for the generation of pharmacological PGP inhibitors.

2 Materials and Methods

2.1 Materials

2.1.1 Chemicals and Reagents

4-(2-hydroxyethyl)-1-piperazineethanesulfonic acid (HEPES)	Carl Roth
4′,6-diamidino-2-phenylindole (DAPI)	Sigma Aldrich
6,8-Difluoro-4-Methylumbelliferyl Phosphate (DiFMUP)	Thermo Fischer
Acrylamide (30 %)	Carl Roth
Aprotinin	Sigma Aldrich
Ammonium persulfate (APS)	Sigma Aldrich
ß-Mercaptoethanol	Sigma Aldrich
Biomol Green (malachite green)	Enzo life sciences
Bis-benzimide trihydrochloride (Hoechst 33342)	Sigma Aldrich
Bleomycin	Sigma Aldrch
Bovine serum albumin fraction V (BSA)	AppliChem
Bromophenol blue	Merck Millipore
Calcium chloride ($CaCl_2$)	Merck Millipore
Dithiothreitol (DTT)	Sigma Aldrich
DMSO (dimethyl sulfoxide)	AppliChem
Dulbecco's modified Eagle's medium (DMEM)	PAN Biotech GmbH
Dulbecco's phosphate buffered saline [(w/o) $MgCl_2$/$CaCl_2$), PBS]	PAN Biotech GmbH
Epidermal growth factor, human (EGF)	Sigma Aldrich
Ethanol	Carl Roth
Fetal calf serum (FCS)	PAN Biotech GmbH
Glacial acetic acid (CH_3CO_2H)	Sigma Aldrich
Glucose	Merck Millipore
Glycerol	AppliChem
Glycine	Carl Roth

Hydrogen peroxide 30 % (H_2O_2)	Sigma Aldrich
Leupeptin	Carl Roth
Magnesium chloride ($MgCl_2$)	AppliChem
Menadione	Sigma Aldrich
Methanol	Carl Roth
N, N, N', N'-tetramethylethylendiamine (TEMED)	Carl Roth
Nonyl phenoxypolyethoxylethanol (NP-40)	Fluka
Para-formaldehyde (PFA)	Carl Roth
Pefabloc SC	Roche
Penicillin G sodium salt	PAN Biotech GmbH
Pepstatin A	Sigma Aldrich
Phosphate standard for Biomol Green	Enzo life sciences
Phosphoglycolic acid lithium salt (PG)	Sigma Aldrich
Phenylmethylsulfonylfluoride (PMSF)	Sigma Aldrich
Ponceau S	Invitrogen
Powdered non-fat milk	Carl Roth
Precision Plus Protein Standard Dual Color	Bio-Rad
Puromycin	Calbiochem
Sodium dodecyl sulfate (SDS), ultra-pure	Carl Roth
sn-Glycerol 3-phosphate bis(cyclohexylammonium) salt (Gro3P)	Sigma Aldrich
Sodium azide (NaN_3)	Merck Millipore
Sodium chloride (NaCl)	Carl Roth
Sodium deoxycholate	Sigma Aldrich
Streptomycin sulfate	PAN Biotech GmbH
Triethanolamine (TEA)	AppliChem
Tris(hydroxymethyl)aminomethane (Tris) base/Tris-HCl	Carl Roth
Triton X-100	Sigma Aldrich
Tween 20	AppliChem

2.1.2 Technical Equipment

Type	Model	Manufacturer
Balance	ACJ 120-4M (10 mg - 120 g)	Kern
Centrifuge	5424 R	Eppendorf
Centrifuge	5804	Eppendorf
Centrifuge	EBA 12R	Hettich
Centrifuge	Universal 16R	Hettich
Counting chamber	Neubauer	Marienfeld
Digital imaging system	ImageQuant LAS 40110	GE Healthcare
Electrophoresis system	Mini-PROTEAN Tetra cell	Bio-Rad
Incubator	BBD 6229	Heraeus
Magnetic stirrer	MR Hei-MixL	Heidolph
Microplate reader	CLARIOstar	BMG Labtech
Microplate reader	EnVision 2104	Perkin Elmer
Microplate reader	SpectraMax Plus 384	Molecular Devices
Microscope	Eclipse Ti-E 2000 (epifluorescence)	Nikon
Microscope	Laborvert FS	Leitz
Microscope	TCS SP5 (confocal)	Leica
Mixer	Unimax 1010 (plate mixer)	Heidolph
Mixer	VORTEX-GENIE 2	Scientific Industries
Multichannel pipettes	Research Plus (0.5-10 µL, 10-100 µL)	Eppendorf
pH meter	Lab 850	Schott Instruments
Pipettes	Research	Eppendorf
Roller mixer	RM 5	A. Hartenstein
Thermomixer	Comfort (1.5 mL)	Eppendorf
Thermomixer	MB-102	Bioer
Transfer cell	Trans-Blot SD semi-dry	Bio-Rad

2.1.3 Consumable Supplies

Type	Model	Manufacturer
96-well plate	Standard F	Sarstedt
96-well plate	MTF	A. Hartenstein
Cell culture dish	Standard 30, 60 & 100 (mm diameter)	Sarstedt
Cell scraper		Biologx
Cell strainer	(70 µm Nylon)	BD Biosciences
Chromatography cellulose	Whatman 3MM	Sigma Aldrich
Concentrator	Pierce, PES (10K MWCO, 0.5 mL)	Thermo Scientific
Falcon tubes	(15 and 50 mL)	BD Biosciences
Fine-ject single use needles	(30 G x 1/2", 0.3 x 12 mm)	Henke Sass Wolf
Fine-ject single use needles	(27 G x 3/4", 0.4 x 20 mm)	Henke Sass Wolf
Nitrocellulose membrane	Hybond C-extra	Amersham
Pipette tips	SurPhob	Biozym
Reaction tubes	(0.5, 1.5 & 2.0 mL)	Eppendorf
Surgical disposable scalpel		B. Braun
Syringe	(1 mL)	BD Plastipak

2.1.4 Commercial Kits

Click-iT EdU Alexa Fluor 488 Imaging Kit	Invitrogen
EnzChek Phosphate Assay Kit (E-6646)	Thermo Scientific
Micro BCA Protein Assay Kit	Thermo Scientific
Pierce LDH Cytotoxicity Assay Kit	Thermo Scientific

2.1.5 Cell Lines

GC1 spg	ATCC

2.1.6 Cell Culture Medium

Complete DMEM		
DMEM supplemented with	4.5 g/L	glucose
	10 %	FCS
	2 mM	L-glutamine
	100 U/mL	penicillin
	100 µg/L	streptomycin
DMEM starving medium		
DMEM supplemented with	4.5 g/L	glucose
	2 mM	L-glutamine
	100 U/mL	penicillin
	100 µg/L	streptomycin

2.1.7 Antibodies

α-Actin mouse monoclonal (clone C4)	Merck Millipore
α-AUM rabbit polyclonal, anti-full-length protein antibodies glycine/magnesium eluate	Charles River, A. Seifried, PhD thesis
α-AUM rabbit polyclonal anti-peptide antibodies	Charles River, P. Duraphe, PhD thesis
α-tubulin mouse monoclonal (DM1A)	Sigma Aldrich
α-rabbit and α-mouse secondary antibodies, HRP-conjugated	Thermo Scientific

2.1.8 Pharmacological Inhibitors

PGP inhibitor #1 (FMP-203794, ChemDiv-2036-0847)	ChemDiv Inc.
PGP inhibitor #2 (FMP-203795, ChemDiv-3289-3526)	ChemDiv Inc.
PGP inhibitor #9 (FMP-208268, ChemDiv-5728-0459)	ChemDiv Inc.
PGP inhibitor #51 (FMP-207031, ChemDiv-4940-1093)	ChemDiv Inc.

2.1.9 Enzymes and Purified Proteins

PGP/PDXP hybrid, recombinant, purified	Elisabeth Jeanclos
Human PGP^{WT}, recombinant, purified	Elisabeth Jeanclos
Murine PGP^{WT}, recombinant, purified	Elisabeth Jeanclos
$PDXP^{WT}$, recombinant, purified	Elisabeth Jeanclos
Trypsin/EDTA	PAN Biotech

2.1.10 Solutions and Buffers

If not stated otherwise, percentages (%) of concentration designate volume per volume (v/v).

SDS-PAGE

Sample buffer (Laemmli's buffer, 4x)	62.5 mM	Tris-HCl
	10 %	Glycerol
	5 %	ß-Mercaptoethanol
	2 %	SDS
	0.02 % (w/v)	Bromophenol blue
		pH 6.8
Running buffer	25 mM	Tris base
	200 mM	Glycine
	1 % (w/v)	SDS
		pH 8.7
Running gel (12 %)	12 % (w/v)	Acrylamide
	0.05 %	APS
	0.003 %	TEMED
	0.1 %	SDS
	375 mM	Tris-HCl
		pH 8.8

Stacking gel	4 % (w/v)	Acrylamide
	0.02 %	APS
	0.002 %	TEMED
	0.1 %	SDS
	125 mM	Tris-HCl
		pH 6.8

Immunoblotting

Anode buffer I	0.3 M	Tris base
	40 %	Methanol
Anode buffer II	25 mM	Tris base
	40 %	Methanol
Cathode buffer	25 mM	Tris base
	40 mM	Glycine
	10 %	Methanol
Blocking buffer	50 mM	Tris-HCl
	2 mM	$CaCl_2$
	80 mM	NaCl
	5 % (w/v)	Powdered milk
	0.2 %	NP-40
	40 %	Methanol
Antibody diluent	10 mM	HEPES
	0.5 M	NaCl
	1 % (w/v)	BSA
	0.2 %	Tween 20
	0.2 % (w/v)	NaN_3
		ph 7.4

Ponceau S solution	0.1 % (w/v)	Ponceau S
	5 %	CH_3CO_2H

Cell lysis and assay buffers

RIPA buffer	50 mM	Tris-HCl
	150 mM	NaCl
	1 %	NP-40
	0.1 % (w/v)	SDS
	0.5 % (w/v)	Sodium deoxycholate
	10 µg/mL	Aprotinin
	10 µg/mL	Leupeptin
	1 mM	Pepstatin
	1 mM	PMSF
		pH 8.0
TMN assay buffer	30 mM	TEA
	5 mM	$MgCl_2$
	30 mM	NaCl
		pH 7.5
TMN lysis buffer	30 mM	TEA
	5 mM	$MgCl_2$
	30 mM	NaCl
	10 µg/mL	Aprotinin
	10 µg/mL	Leupeptin
	1 mM	Pepstatin
	1 mM	Pefabloc SC
		pH 7.5

2.1.11Software

GraphPad Prism 5.0	GraphPad Software
Image-Pro software 7.0	Media Cybernetics
MARS Data Analysis Software 3.20 R2	BMG Labtech
SoftMax Pro 6.2.2	Molecular Devices

2.2 Methods

2.2.1 Cell Culture Techniques

2.2.1.1 Cell Lines

For the investigation of PGP-mediated cellular effects murine spermatogonial cells named GC1-spg (from now on referred to as GC1 cells) were used. PGP is a ubiquitous enzyme, and highly expressed in testicular germ cells. For the experiments via RNA interference PGP depleted shRNA cells, and control shRNA cells were used (Seifried et al., 2014). Figure 9 shows the amount of endogenous PGP reduction. These cells were maintained in cell culture dishes in Complete DMEM containing 1 µg/mL puromycin at 37°C and 7 % CO_2 in a humidified cell incubator.

2.2.1.2 Thawing Cells

Frozen cells were kept in tanks of liquid nitrogen. After removal from the tanks the cells were thawed at 37°C in a water bath. When only a little ice crystal remained in the vial, the cell suspension was resuspended, added to 9 mL preheated Complete DMEM and centrifuged for 5 minutes at room temperature and 250 x *g*. After discarding the supernatant, the pellet was resuspended in 1 mL Complete DMEM and pipetted into a 10 cm dish with 9 mL of preheated medium. The medium was changed 24 hours later.

2.2.1.3 Transfection with Human PGP

The transfection of PGP shRNA cells with Lipofectamin 2000 was performed by Gabriela Segerer. PGP shRNA cells, i.e. PGP-depleted murine GC1 cells, were transfected

with 140 ng of RNA interference-insensitive human PGP^{WT} tagged with tdTomato (a fluorescent protein for controlling the successful transfection) to receive approximately the same amount of PGP in comparison to control shRNA cells (figure 9) (Segerer, 2015, Segerer et al., 2018).

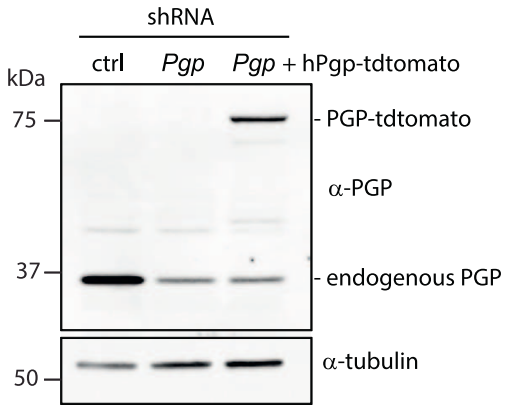

Figure 9. PGP expression levels in the indicated cell types. *Blots were reprobed with α-tubulin antibodies to assess protein loading. The figure was produced by Gabriela Segerer and published in (Segerer et al., 2018). Copyright Elsevier.*

2.2.2 Protein Analytics

The amount of PGP in cellular lysates was quantified by gel electrophoresis and Western Blot analysis.

2.2.2.1 Cell Lysis and Sample Preparation

Table 1. Different concentrations of oxidative stress inducing substances and their incubation times (for each concentration).

Substance	Concentration	Incubation time
Bleomycin	1 µg/mL and 10 µg/mL	12 h
EGF	400 ng/µL	3 min
H_2O_2	0.1 mM, 1 mM, and 10 mM	2 min

GC1 control shRNA cells were exposed to oxidative stress inducing reagents (table 1). The incubation was immediately stopped by removal of the supernatant and washing with 1 mL isotonic NaCl. After discarding the NaCl, 250 µL of ice-cold RIPA lysis buffer was added. The cells were detached using a cell scraper, the lysates were then transferred into 1.5 mL reaction tubes. The cells were lysed by repeatedly shearing through needles of 0.3 mm diameter (30 x *g*). Nuclei and cell debris were removed by centrifugation for 15 minutes at 4°C and 21.130 × *g* (15,000 rpm). The supernatant was subsequently transferred into new reaction tubes and kept on ice.

For the sample preparation the amount of protein was determined according to BCA evaluation with the Micro BCA Protein Assay Kit (Thermo Scientific). The plate was kept in an incubator at 37°C for 20 to 60 minutes, then the absorbance was measured at 562 nm in the SpectraMax Plus (Molecular Devices). The protein amount was compared to a BSA standard curve (0, 2, 4, 6, 8, 10 µg BSA per well) after subtraction of the buffer's background. The lysates were mixed with 4 x Laemmli's sample buffer (Laemmli, 1970) according to the amount of protein in the lysates to receive the same total amount of protein.

2.2.2.2 Sodium Dodecyl Sulfate Polyacrylamide Gel Electrophoresis (SDS-PAGE)

SDS-PAGE enables the separation of proteins according to their molecular mass. The proteins were boiled in SDS-PAGE sample buffer for 3 minutes and thus denatured. For PGP (ca. 34 kDa) a 12 % gel was used, that sorts proteins of low to medium molecular weight (Laemmli, 1970). The gel plates were fixed in a gel chamber that was filled with running buffer. 3.5 µL of Precision Plus Marker were pipetted into the first (left) well. Subsequently the other wells were loaded with samples as required. The protein concentration in the stacking gel was conducted at 75 V, 3 A and 300 W for 15 minutes; the protein separation in the running gel was conducted at 150 V, 3 A and 300 W until the samples reached the end of the gel.

2.2.2.3 Western Blot Analysis

After their separation, the proteins were transferred semi-dry onto a nitrocellulose membrane for western blot analysis. Two sheets of Whatman paper soaked in anode buffer I and another one soaked in the anode buffer II were stacked on the blotting machine. The membrane was soaked in H_2O_{dest}, shortly placed in anode buffer II and then put on top of the filter papers. The SDS-PAGE gel wetted in cathode buffer was placed thereupon. The three sheets of Whatman paper soaked in cathode buffer were also stacked. Proteins were blotted for one hour at 70 mA (1 blot) and 25 V constantly. The protein transfer was verified by staining with Ponceau S.

To avoid unspecific binding of proteins the membrane was blocked in blocking buffer for 15 minutes and thereby continuously shaken. It was washed in H_2O_{dest} and incubated with primary antibodies on a roller mixer overnight at 4°C (α-AUM; diluted 1:1,000 in antibody diluent) or for three to four hours at room temperature (α-tubulin; diluted 1:10,000 in antibody diluent). After rinsing with H_2O_{dest} the next day, the membrane was incubated with horseradish peroxidase (HRP)-labelled secondary antibodies (diluted 1:10,000 in blocking buffer) for one hour. Super Signal West Pico Stable Peroxide Solution and Luminol/Enhancer Solution were mixed 1:1 and the blot was developed therein for 3 minutes. ImageQuant LAS 4010 Digital Imaging System was used for the detection of protein signals.

2.2.3 Cellular Assays

2.2.3.1 Cytotoxicity Assay

To quantify cytotoxicity of the different inhibitors and oxidative stress inducing agents the lactate dehydrogenase (LDH) release was measured with the Pierce LDH Cytotoxicity Assay Kit (Thermo Scientific). The ubiquitous cytosolic enzyme LDH is released into the cell culture medium in case of plasma membrane damage. The amount of released LDH can be determined by a coupled enzymatic reaction. NAD^+ is reduced to NADH by the LDH catalyzed oxidation of lactate to pyruvate. This NADH can be then oxidized by diaphorase to transform a tetrazolium salt (INT) into a red formazan which can be measured at 490 nm. (Korzeniewski and Callewaert, 1983)

For each condition 3,000 of control shRNA and 3,500 of PGP shRNA GC1 cells were seeded on a 96 well plate in duplicates in growing conditions and kept in a humidified cell culture incubator at 37°C and 7 % CO_2.

The substances were solved in Complete DMEM and added as listed in table 2 (200 µL per well). Whenever the inhibitors were solved in DMSO a control with the same amount of DMSO as in the inhibitor dilution was performed.

The LDH release then was determined according to the manufacturer's instructions.

Compound concentrations that caused an LDH release above 21 % were not used for incubation of cells.

Table 2. Different concentrations and incubation times of substances for the quantification of their cytotoxicity.

Substance	Concentration	Incubation time
Bleomycin	2.5 µg/mL	17h
H_2O_2	1 mM and 0.1 mM	17h and 1h
Menadione	10 µM, 5 µM and 1 µM	17h and 45 min
PGP inhibitor #1	10 µM and 50 µM	3h
	50 µM and 200 µM	1h
PGP inhibitor #2	30 µM and 50 µM	3h
	50 µM and 200 µM	1h
PGP inhibitor #9	20 µM and 50 µM	3h
	50 µM and 200 µM	1h

2.2.3.2 Proliferation Assay

Effects on cellular proliferation were investigated with the Click-iT EdU Alexa Fluor 488 Imaging Kit (Invitrogen). The treated cells incorporate EdU (5-ethynyl-2'-deoxyuridine) and integrate it into their DNA during DNA replication, i.e. proliferation. The number of nuclei that integrated EdU can be registered by the help of a fluorescence microscope and quantitatively compared to the total number of nuclei marked by the DNA intercalator Hoechst 33342.

On day one, 3,000 GC1 cells (control and PGP shRNA) were seeded in 200 µL of Complete DMEM containing puromycin per well on a 96 well plate in duplicates for each condition. Then they were stored in a humidified cell incubator at 37°C for several hours till they attached. Afterwards, the adherent cells were exposed to different conditions (for the incubation time of 17 hours; table 3), the shorter incubated cells were treated on day two (prior to the addition of EdU).

Therefor the mentioned concentrations were prepared in Complete DMEM (including puromycin) and the medium was changed subsequently; for the non-treated cells an exchange into fresh medium (if not mentioned otherwise, this means Complete DMEM containing puromycin) was performed. The cells were maintained in the humidified cell incubator at 37°C after the particular treatment.

Table 3. Different concentrations of oxidative stress-inducing agents and inhibitors with their incubation times before addition of EdU (implying prolonged incubation for 2.5h).

Substance	Concentration	Incubation time
Bleomycin	2.5 µg/mL	17 h
EGF	100 ng/mL	together with EdU
H_2O_2	0.1 mM	1 h*
Menadione	1 µM or 10 µM	17 h or 45 min*
NAC	10 mM	1 h
PGP inhibitor #1	10 µM, 20 µM, 50 µM, and 200 µM	1 h

** The incubation with menadione and H_2O_2 was stopped after 45 and 60 minutes respectively by an exchange into fresh medium. These cells were kept overnight, and the proliferation was assayed together with the cells incubating for 17h with the indicated substances.*

After the indicated time the quantification of DNA synthesis was started by addition of 10 µM EdU. The cells were incubated for another 2.5 hours at 37°C. After fixation and permeabilization the cells incorporating EdU and the DNA (stained with the DNA intercalator Hoechst 33342) as reference were stained as recommended by the manufacturer.

Imaging was performed by a Nikon Ti-E Eclipse epifluorescence microscope at 10 x magnification. For analysis Image Pro Software 7.0 and GraphPad Prism were used.

2.2.4 Protein Expression and Purification

Protein expression and purification was performed by Elisabeth Jeanclos according to the protocol published by Annegrit Seifried (Seifried, 2014). For completeness and comprehensibility, the procedure is briefly described in the following.

His_6-tagged murine and human PGP^{WT} was overexpressed in *E. coli* BL21 (DE3) (pG-Tf2). Cells were lysed after 20 hours, or after 18 hours for the PGP/PDXP hybrid. Cleared bacterial lysates were loaded onto a Ni-NTA agarose column with His Trap coupled to an ÄKTApurifier FPLC system to washout unbound proteins. The sample was eluted using a linear 10-400 mM imidazole gradient.

The peak fractions were tested for phosphatase activity towards Para-nitrophenylphosphate (pNPP). pNPP is an artificial dephosphorylation substrate which allows continuous detection of phosphatase activity. The hydrolysis product para-nitrophenolate can be colorimetrically measured at 405 nm under alkaline conditions.

The active fractions were pooled and concentrated and afterwards exposed to tobacco etch virus protease for cleavage. Uncleaved protein was separated from cleaved protein and the His-tagged protease. Active fractions containing untagged protein were again pooled and concentrated. The purity control was conducted by SDS-PAGE and Coomassie Blue staining.

2.2.5 Phosphatase Activity Assays

All phosphatase activity assays presented in this work were conducted in 96 well microtiter plates. The measurement was evaluated, and kinetic constants were calculated (from data fitted by nonlinear regression to the Michealis-Menten equation) using GraphPad Prism.

2.2.5.1 Dephosphorylation of PG (Malachite Green Assay)

Lately, PG was detected to be a highly specific substrate of PGP (Segerer et al., 2016). The hydrolysis product glycolate cannot be directly measured. So dephosphorylation of PG must be quantified indirectly via the detection of the released inorganic phosphate (P_i). The here used Biomol Green Reagent (Enzo) is an advancement of the classic malachite green assay. In principle, molybdate reacts with the P_i, phosphomolybdate then complexes with malachite green, a cationic dye, that yields a detectable absorbance maximum between 600 and 680 nm (Itaya and Ui, 1966).

For the following assays a reaction volume of 50 µL with TMN with 0.01 % Triton as assay buffer was used. The buffer was always supplemented with 4 mM DTT except for the analysis of PGP activation by reduction. The activity was stopped after indicated time points by addition of 100 µL of Biomol Green Reagent (Enzo). The plate was incubated for 10 to 15 minutes at room temperature, then the absorbance was measured at 620 nm in the EnVision 2104 multilabel microplate reader (Perkin Elmer). The phosphate release was quantified by standard curves.

2.2.5.1.1 Experiments with Purified Protein

Effect of Reduction on PGP Activity

This assay should enable the analysis of kinetics and reevaluate the activating effect of DTT on PGP (Seifried et al., 2016). Highly concentrated recombinant murine PGP^{WT} was prepared to receive a final amount of 0.04 µg per well and incubated in buffer with or without 5 mM DTT for 20 minutes at room temperature (around 22°C in the primary cell culture).

Table 4. Concentrations of substrate PG in the working solution and in the assay.
Concentrations in µM.

PG in substrate dilution	4000	2000	1000	500	250	125	62.5	31.25
PG in total volume	800	400	200	100	50	25	12.5	6.25

Meanwhile, the substrate was diluted serially from 800 to 6.25 µM in a final volume of 50 µL per well. Next the substrate dilutions were distributed on a 96 well plate in duplicates (10 µL per well). As start of reaction 40 µL of buffer or enzyme dilution (with or without DTT respectively) were added to every well. The reaction was stopped after 4 minutes with Malachite Green.

Kinetics for Human and Murine PGP and the PGP/PDXP Hybrid

Here, only 0.01 µg of highly concentrated murine and human PGP^{WT} was used per well. The enzymes and the buffer control incubated for 10 to 15 minutes at room temperature. Meanwhile the PG dilution was prepared and distributed similar to the description above. The reaction then was started by addition of the enzyme mixtures and stopped with Malachite Green after 3 minutes.

The activity assay with the PGP/PDXP hybrid was performed by the use of 0.884 µg of protein per well in TMN assay buffer with 5 mM DTT and substrate dilutions from 2000 to 31.25 µM in a final volume of 50 µL per well. The reaction was stopped after 5 minutes.

Inhibitor Studies

The inhibitory effect of the compounds screened by the FMP (by the use of 6,8-difluoro-4-methylumbelliferyl phosphate (DiFMUP) as an artificial substrate) should then be tested and evaluated for the physiological activity of PGP against PG.

The assay was performed with 0.01 µg of highly concentrated recombinant murine or human PGP^{WT} per well. For the concentration-response analysis the PG concentration was constant at 200 µM and the different inhibitors were prepared in a twofold serial dilution (tables 5 and 6). For #1 concentrations from 32 to 0.0078125 µM in a final volume of 50 µL and for #2 and #9 from 64 to 0.015625 µM were used. Because of a limited number of wells on each plate the second lowest and the fourth highest concentrations were not tested.

Table 5. Concentrations of inhibitor #1 in working solutions and in assays with murine and human PGP.
Concentrations in µM.

in serial dil.	160	80	40	10	5	2.5	1.25	0.625	0.3125	0.15625	0.0390625
in total volume	32	16	8	2	1	0.5	0.25	0.125	0.0625	0.03125	0.0078125

Table 6. Concentrations of inhibitors #2 and #9 in the working solutions and in the assay with murine and human PGP and of #1 for the PGP/PDXP hybrid assay.
Concentrations in µM.

in serial dilution	320	160	80	20	10	5	2.5	1.25	0.625	0.3125	0.078125
in total volume	64	32	16	4	2	1	0.5	0.25	0.125	0.0625	0.015625

For the inhibition of the PGP/PDXP hybrid 0.884 µg of protein per well in TMN assay buffer with 5 mM DTT, 500 µM of PG and 5 minutes of reaction time were applied. The inhibitors were all diluted serially from 64 to 0.015625 µM in TMN with 0.01 % Triton.

For kinetic measurements, the substrate concentrations ranged from 800 to 12.5 µM (600 µM additionally) whereas the inhibitor concentrations were settled around the IC_{50} from 2 to 0.125 µM for #1 and from 8 to 0.5 µM for #2 and #9. The solutions were prepared serially.

First, the enzyme was added to the buffer. Then, the inhibitor dilutions were prepared and distributed on a 96 well plate (10 µL per well). The control without inhibitor contained only buffer. The enzyme mix (30 µL per well) was added to the inhibitor and the plate was incubated for 15 minutes at room temperature protected from light. Then the reaction was started by addition of substrate (10 µL per well) and stopped with Malachite Green after 3.5 minutes for concentration-response and after 3 minutes for kinetics.

2.2.5.1.2 Experiments with Cellular PGP

The following assay was performed to analyze modifications in PGP's phosphatase activity due to different conditions.

Lysates of GC1 Cells

A Complete DMEM suspension with 1 million GC1 cells (for each dish, i.e. control cells for different treatments, PGP shRNA cells and/or PGP shRNA cells transfected with human PGP) in a 15 mL falcon was prepared on the basis of counting on a Neubauer chamber. The falcons were centrifuged for 4 minutes at 22°C and 88 x *g* (1090 rpm). In the following the supernatant was removed, the pellet was resuspended in 1 mL of isotonic sodium chloride (NaCl) and centrifuged again as stated above. The washing was repeated. After discarding the supernatant, the cells were resuspended in 250 µL of ice-cold hypotonic TMN lysis buffer and transferred into 1.5 mL reaction tubes. The cells were lysed by repeatedly shearing through needles of 0.3 mm diameter (30 x *g*). To separate the intracellular liquid with proteins from the heavier membrane and nucleus, the cells were centrifuged for 15 minutes at 4°C and 21.130 × *g* (15,000 rpm). The supernatant was subsequently transferred into new reaction tubes and kept on ice. The lysates were utilized for cellular assays within a few hours.

When the cells were exposed to oxidative stress, 1 million cells were seeded on 6 cm dishes in the morning. After adhesion, the medium was changed in the afternoon to DMEM starving medium. The dishes were incubated overnight at 37°C in the cell incubator.

Oxidative stress inducing reagents were added in the next morning for defined time periods: H_2O_2 (0.1 mM for 0, 2, 5 and 10 minutes) and menadione (1 µM for 0, 15, 30, and 45 minutes).

The incubation was immediately stopped by removal of the supernatant and washing with 1 mL isotonic NaCl. After discarding the NaCl, 250 µL of ice-cold TMN lysis buffer was added. The cells were solved by the thorough use of a cell scraper, the lysates were then transferred into 1.5 mL reaction tubes. Cell lysis and centrifugation was performed as described above. The lysates were kept on ice.

Assay

The reaction mixtures were prepared as follows (tables 7 and 8; first without substrate) in 1.5 mL reaction tubes (a pair of reaction assay and background/reference assay without substrate for each lysate) at room temperature. Assays evaluating the impact of oxidative stress were performed in the absence of DTT (because it is a reducing agent; table 8).

Table 7. Composition of reaction mixture for the PGP activity assay with GC1 cell lysates.
For this assay lysates derived from control cells, PGP shRNA cells and PGP shRNA cells transfected with human PGP (Rescue). DTT (dithiothreitol) as activator, PG (phosphoglycolate) as substrate, TMN (TEA/triethanolamine, $MgCl_2$ and NaCl) as reaction buffer.

Compound	with substrate	without substrate
TMN	231 µL	261 µL
$MgCl_2$ 250 mM	6 µL	6 µL
DTT 1 M	3 µL	3 µL
Lysate	30 µL	30 µL
PG 10 mM	30 µL	0 µL

Table 8. Composition of reaction mixture for the PGP activity assay with GC1 cell lysates.
For this assay lysates deriving from control cells were pretreated with oxidative stress inducing agents H_2O_2 and menadione. PG (phosphoglycolate) as substrate, TMN (TEA/triethanolamine, $MgCl_2$ and NaCl) as reaction buffer.

Compound	with substrate	without substrate
TMN	117 µL	132 µL
$MgCl_2$ 250 mM	3 µL	3 µL
Lysate	15 µL	15 µL
PG 10 mM	15 µL	0 µL

30 µL of TMN were pipetted into each required well on a 96 well plate. 20 µL of the specimen were pipetted in duplicates on the plate for each time point and the reaction was immediately stopped by the addition of Malachite Green. Meanwhile the reaction tubes were incubated at 37°C in a thermomixer.

Determination of Protein Concentration with the BCA Assay

For further calculation of PGP activity (reaction velocity) the amount of protein was determined according to BCA evaluation with the Micro BCA Protein Assay Kit (Thermo Scientific). In alkaline environment, proteins reduce Cu^{+2} to Cu^{+1}. One Cu^{+1} ion can chelate with two bicinchoninic acid (BCA) yielding to a colorimetrically measurable complex (the

color intensity corelates with the protein concentration) (Smith et al., 1985). The plate was kept in an incubator at 37°C for 20 to 60 minutes, then the absorbance was measured at 562 nm in the SpectraMax Plus (Molecular Devices). The protein amount was compared to a BSA standard curve (0, 2, 4, 6, 8, 10 µg BSA per well) after subtraction of the buffer's background.

2.2.5.2 Dephosphorylation of Gro3P (EnzChek Phosphate Assay)

Another substrate of PGP is Gro3P (Mugabo et al., 2016). Since the affinity of PGP towards Gro3P and thus the detectable P_i release is much lower than towards PG, a more sensitive assay is necessary. With the EnzChek Phosphate Assay Kit (Thermo Scientific) P_i can be detected between 2 to 150 µM by a coupled enzymatic reaction. The kit product MESG (2-amino-6-mercapto-7-methylpurine riboside) is converted to ribose 1-phosphate and 2-amino-6-mercapto-7-methylpurine by PNP (purine nucleoside phosphorylase) which results in a change of the absorption maximum.

Inhibitor Studies

To determine whether the inhibitory effect also appeared towards the dephosphorylation of the other physiological substrate of PGP Gro3P, #1 was used exemplarily.

All reagents were prepared to receive a total volume of 100 µL per well (table 9). Purified murine PGP^{WT} was diluted in TMN assay buffer (containing 0.01 % Triton and 5 mM DTT) to get 1 µg of protein in 24 µL per well. Buffer alone was used as control. Inhibitor #1 was prepared in a serial dilution in TMN with 0.01 % Triton with concentrations ranging from 32 to 0.0078125 µM in the final volume (see also table 5) and distributed on a 96 well plate (20 µL per well). The buffer mix was incubated on the 96 well plate for 15 minutes at room temperature protected from light. The EnzChek reagents incubated with the substrate Gro3P in 1.5 mL reaction tubes for 10 minutes under the same conditions. After incubation, the reaction was started by addition of the EnzChek substrate mix with a multichannel pipette and the absorption was immediately recorded in the CLARIOstar prewarmed to 37°C at 330 nm (detection of MESG decrease) and 360 nm (detection of phosphate release by increasing EnzChek product amounts)

every minute for 30 minutes. The time point for calculation was chosen within linearity of the reaction, here 7 minutes.

Table 9. Composition of reaction components for detecting Gro3P dephosphorylation by purified PGP in the presence of inhibitor #1.
Gro3P (glycerol-3-phosphate) as substrate. 100 µL total reaction volume.

Assay components	per well	final concentration
Buffer mix (protein + inhibitor + buffer)	44 µL	
EnzChek mix	26 µL	
Gro3P 5 mM	30 µL	1.5 mM

2.2.6 Data Analysis

The number of independent experiments is always stated in the respective legend. GraphPad Prism 5.0 was used for data analysis. The data are given as mean values ± S.E.M. Unpaired Student's t-tests were performed for explorative statistical analysis of differences between two groups. P-values were considered as statistically significant in the following range: *p<0.05; **p<0.01; ***p<0.001. Data from kinetic measurements were fitted by nonlinear regression to the Michealis-Menten equation. Data from concentration-response inhibition measurements were fitted by nonlinear regression to the log(inhibitor) vs. response equation.

3 Results

3.1 Effect of ROS on PGP Activity and PGP-dependent Proliferation

Depending on the dose of ROS and other reactive oxidants oxidative stress ranges from physiological signaling and regulation processes (also termed “oxidative eustress”) to pathophysiological consequences (also termed “oxidative distress”) (Sies et al., 2017).

Purified PGP can be reversibly inhibited by oxidation (see 1.3.4.1), supposedly as a feature of physiological EGF-related ROS signaling (Seifried et al., 2016). In addition, it has been assumed that PG is released as a result of oxidative DNA damage (see 1.3.2.1) and PGP downregulated cells might proliferate less due to the inability to dephosphorylate increased levels of PG.

Here, the effect of different oxidants (and an antioxidant) on cellular PGP activity and PGP-dependent proliferation was investigated. Western Blot analysis verified beforehand that incubation with ROS producing agents such as bleomycin (BLM), epidermal growth factor (EGF), and H_2O_2 caused no remarkable alteration in PGP expression in GC1 control shRNA cells (figure 10).

In aerobic cells, superoxide anion radicals are regularly formed from molecular oxygen through autooxidation or enzymatic reactions (Sies et al., 2017). These radicals are usually converted by superoxide dismutases or spontaneously into the more stable H_2O_2 (Sies et al., 2017). H_2O_2 is a nonradical within the ROS that are in general radical and

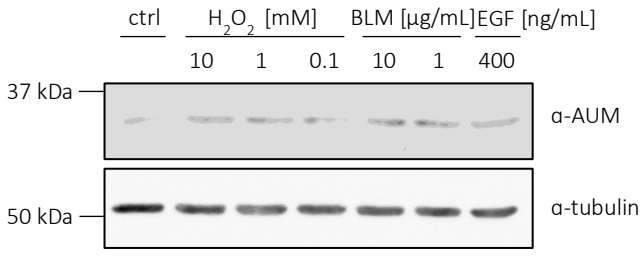

Figure 10. Unaltered PGP expression in lysates of GC1 cells upon oxidant treatment.
PGP ctrl shRNA cells were exposed to the indicated substances (H_2O_2 for 2 min, BLM for 17 h, EGF for 3 min) before lysis (ctrl = control, BLM = bleomycin, EGF = epidermal growth factor). The lysates were immunoblotted with a α-PGP antibody. PGP expression in non-treated control cells was used as standard, tubulin expression was detected as loading control. Result of one preliminary experiment.

nonradical reactive reduction products of molecular oxygen (Sies et al., 2017). For example, in liver H_2O_2 production reflects 2 % of the O_2 uptake (Sies et al., 2017). Physiological concentrations range around 10 nM that vary in different cellular compartments and metabolic situations (Sies et al., 2017). For experiments, H_2O_2 is well suited because it is stable and uncharged (and thus easily passes the plasma membrane to enter the cell), but also a very potent oxidant (Rhee et al., 2000, Sies et al., 2017). Depending on the concentration it can oxidize proteins to mimic pro-proliferative signaling processes (ca. 10 nM - 1 µM) or cause damage to DNA and other cellular components (Burdon, 1995). However, concentrations (0.1 - 0.5 mM) resulting in significant DNA damage still do not have to be lethal (Driessens et al., 2009).

Extracellular binding of EGF to the transmembrane receptor EGFR can induce signaling cascades that affect cellular proliferation, differentiation and apoptosis (Berg et al., 2018). Of note, EGFR can also be activated by other ligands with higher or lower affinity and without ligand-binding (e.g. by irradiation or exogenous H_2O_2) in order to modulate signaling effects and thus exerts multiple and diverse biological processes (Zeng and Harris, 2014). Activated (here EGF-bound) EGFR can induce the production of H_2O_2 as messenger which oxidizes e.g. PTPs (Rhee et al., 2000). Their so-achieved inactivation can be related to phosphorylation and activation of protein tyrosine kinases downstream in EGFR signaling (Rhee et al., 2000). EGF-mediated processes are overall tightly connected with and presumably fine-tuned by (transient) redox regulation of EGFR itself and its cooperation partners (Heppner and van der Vliet, 2016). Also, redox regulated PGP seems to be involved in EGF signaling (Seifried et al., 2016, Segerer et al., 2018).

Menadione (2-methyl-1,4-naphthoquinone, MN) can be processed by one-electron reduction into a semiquinone radical, which can oxidize intracellular O_2 forming ROS as well as low molecular weight thiols such as glutathione and protein thiols (referred to as redox cycling). Protein thiols can also be oxidized secondarily by MN-induced ROS. Quinones can furthermore act as electrophiles and inactivate enzymes by covalent binding to functional nucleophiles. Low concentrations of MN (50-100 µM) are supposed to activate EGFR signaling and thus proliferation via thiol oxidation (or binding) of

phosphatases antagonizing EGFR signaling (in rat hepatocytes). Upon application of higher concentrations (200 µM and more) thiol oxidation increases drastically and might account for the loss of cell viability. Levels of intracellular reduced glutathione (as main representative of soluble thiols) decrease relative to applied MN concentrations which impairs the resistance to oxidative threats (as it might prevent or delay effects on protein thiols). Furthermore, MN can induce DNA damage via binding of the semiquinone radical to DNA or ROS generation (e.g. in rat hepatocytes and human HaCaT keratinocytes). (Di Monte et al., 1984, Morrison et al., 1984, Klotz et al., 2014)

Bleomycin (BLM), a glycopeptide-derived antibiotic, is used as cytostatic drug in cancer therapy as it can specifically induce oxidative DNA damage to one or both strands. The peptide containing a pyrimidine and a bithiazole can directly bind to DNA at dedicated recognition sites. A metal ion, mostly iron(II) (Fe^{2+}) necessary for DNA strand scission is bound to the pyrimidine-imidazole section. When Fe^{2+}·BLM complexes O_2, it is activated via one electron reduction (by any available reductant). The resulting high valent iron oxyl can form a C-4' sugar radical. The electron from the radical can be transferred onto an O_2 which will induce the cleavage of the C(3')-C(4')-bond within the DNA and leave a base propenal and a 3'-PG end. Notably most DNA-cleaving radicals stay bound to BLM, whereas hydroxyl radicals are formed only in small, biologically unimportant amounts. (Stubbe and Kozarich, 1987, Breen and Murphy, 1995)

3.1.1 Influence of Different Oxidants on Cellular PGP Activity

Exposure of GC1 cells to oxidants for quite short incubation times before lysis should directly affect PGP conformation and/or activity. GC1 cells were incubated with H_2O_2 or MN for a few minutes and then lysed. Subsequently, the enzymatic activity of PGP from the lysates was measured against the physiological substrate PG. The assay was stopped and evaluated after 15 minutes.

PGP activity is significantly reduced after incubation with H_2O_2 for 5 minutes. This activity decrease is normalized after an incubation for 10 minutes (figure 11A). Hence, oxidation and inhibition of PGP in the observed cells is reversed by intracellular reducing processes within minutes after H_2O_2 addition.

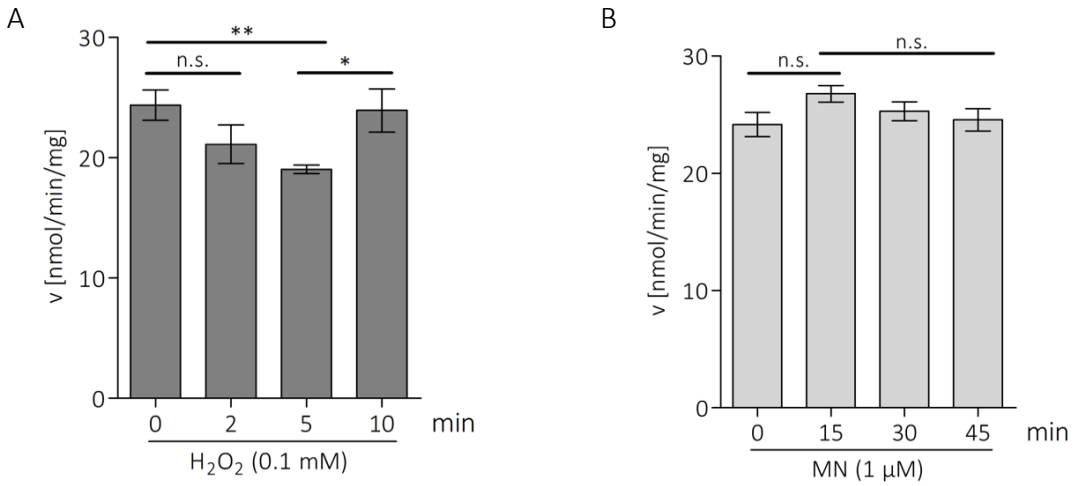

Figure 11. Change of cellular PGP activity upon oxidative stress.
*Incubation with the oxidants H_2O_2 (A) and menadione (B). The activity was measured after 15 minutes (A) or 30 minutes (B). Results are mean ± SEM of n=4 (A) or n=3 (B) independent experiments. n.s. = not significant; *p<0.05; **p<0.01.*

Short time incubation with menadione seems to elevate the amount of released phosphate (p = 0.1037, although this trend did not reach statistical significance), which is again normalized after longer treatment duration (p = 0.1358; figure 11B). ROS production by MN takes longer because MN has to be processed first. This is also the reason why a longer incubation period was chosen. Apparently, ROS produced by incubation of cells with MN do not oxidize PGP and therefore do not inhibit it. The activation could be due to other compensatory processes. Or the effect may originate from the dosage and H_2O_2 was applied in much higher concentrations than MN. So that in fact ROS would activate PGP in very low concentrations and all H_2O_2 observations would be the result of excessive oxidation.

3.1.2 Possible Impact of PGP's Redox-sensitivity on Cellular Proliferation

On the one hand PGP is sensitive to reversible oxidation (supposedly, an effect of ROS signaling as "oxidative eustress") (Seifried et al., 2016), on the other hand the PGP substrate PG is (at least to some extent) derived from oxidative DNA damage (an effect of "oxidative distress") (Fung and Demple, 2011, Iyama and Wilson, 2013). Furthermore, an oxygen dependent proliferation deficit was observed in PGP depleted or inactivated cells (Segerer et al., 2016). To better understand possible connections, PGP shRNA and

control cells were treated with various oxidants and their effects on proliferation were analyzed.

3.1.2.1 Impact of PGP Downregulation and Rescue on Cellular PGP Activity and Proliferation

Downregulation of PGP expression via shRNA to about 20 % of remaining protein in the examined GC1 cells (see 2.2.1.1 and figure 9) is a well-established working model (Seifried et al., 2014, Segerer, 2015, Segerer et al., 2018). Whether PGP activity could also be reduced congruently was quantified within the present work (and already published in (Segerer et al., 2018)). After 30 minutes lysates of control shRNA cells had dephosphorylated approximately 4.1 times more PG as lysates of PGP shRNA cells (figure 12A). Hence, PGP shRNA cells lack PGP activity what might account for metabolic disturbances.

In the next step it was interesting to rescue PGP in the downregulated murine cells. PGP shRNA cells were transfected by Gabriela Segerer with interference-resistant human PGP^{WT} to endogenous PGP expression levels (see 2.2.1.3 and figure 9). Lysates of these rescue cells had released ca. 2.6 times as much P_i from PG after 15 minutes compared to the control (figure 12A), which fits the slightly lower K_M of human compared to murine PGP (see also figure 16A and table 11). Thus, rescuing PGP activity in PGP shRNA cells is possible and even results in a notable activity increase.

Recent studies already demonstrated constantly decreased proliferation of PGP inactive or deficient cells (Segerer et al., 2016, Segerer, 2015). It should be figured out whether transfection of PGP shRNA cells with human PGP would also rescue the proliferation defect. Proliferation assays were performed with GC1 cells in culture by determining the number of EdU-incorporating cells across various treatments. The assay allows to measure DNA replication counting nuclei that integrated EdU compared to the total number of nuclei. PGP depleted cells were always compared to control cells with normal PGP activity (figures 9 & 12A). Within 2.5 hours PGP shRNA cells incorporated constantly 8.88 % less EdU than control cells (figure 12B) which expresses their proliferation defect as expected. However, the proliferation of PGP shRNA cells could only

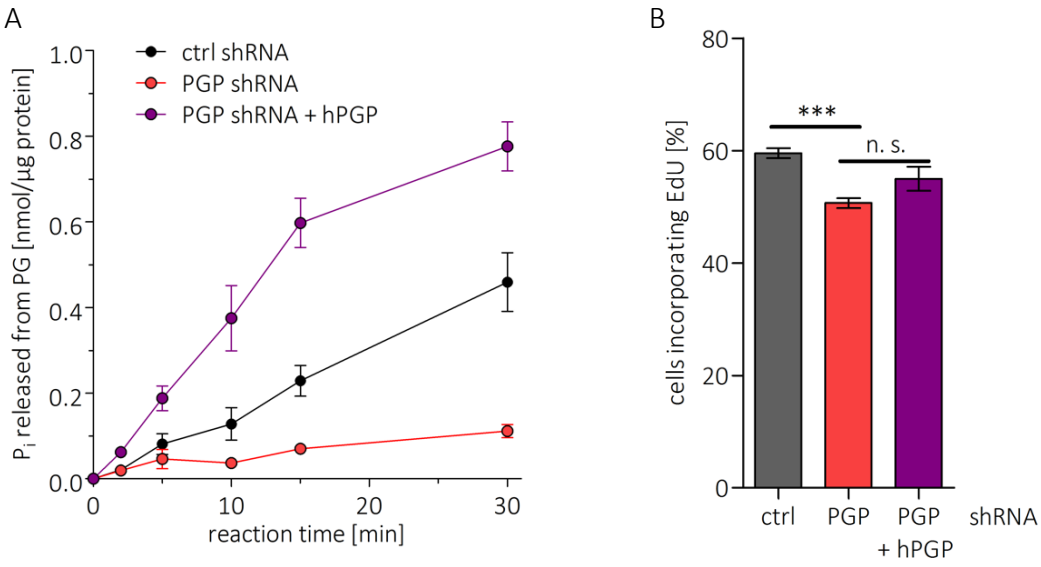

Figure 12. Changes in cellular PGP activity and proliferation in downregulated cells and the rescue with human PGP compared to control cells.

(A*) PGP activity assay in GC1 cell lysates. Free phosphate released from exogenous PG was measured using malachite green. The data represent mean values ± S.E.M. of n=5 (PGP shRNA + hPGP) or n=6 (control and PGP shRNA) replication experiments. Error bars not seen are hidden behind the symbols. The results and the figure are already published in (Segerer et al., 2018). Copyright Elsevier. (B) Effect of PGP shRNA and transfection of PGP shRNA cells with interference-resistant human PGP on cell proliferation. 3,000 GC1 cells were seeded per well. Proliferation was measured by quantification of the cells that incorporated EdU within 2.5 additional hours (i.e. also additional incubation time) and compared to the number of nuclei stained with Hoechst. The results represent mean values ± S.E.M. of n=4 (PGP shRNA + hPGP) or n=18 (ctrl & PGP shRNA) independent experiments. ***p<0.001.*

be elevated to 54.97 % after transfection with human PGP which means a not statistically significant increase of 4.31 % (p = 0.0596, remaining difference to control shRNA = 4.57 %). Hence, it was not possible to totally rescue proliferation here. It is not clear whether the murine and human enzyme have the same metabolic functions. Additional experiments might be desirable.

3.1.2.2 Cytotoxicity Control for ROS Producing or Neutralizing Compounds

Before exposing the cells to the different ROS producing (BLM, H_2O_2, MN, and EGF) or neutralizing (NAC) compounds, they needed to be checked for cytotoxicity. Of course, cytotoxic agents would reduce cellular proliferation. EGF is not supposed to be cytotoxic because of its physiological role (Zeng and Harris, 2014). The reducing agent N-acetylcysteine (NAC) is reported to have a relatively low cytotoxicity (Samuni et al., 2013). Bleomycin (BLM), H_2O_2, and menadione (MN) are known to be cytotoxic beyond certain

concentrations (Di Monte et al., 1984, Stubbe and Kozarich, 1987, Driessens et al., 2009). In order to control for this effect, the concentrations of the compounds were chosen below a cytotoxicity level of 21 % which was assessed by the measurement of LDH release. LDH is a cytosolic enzyme which can be detected in the cell medium in case of plasma membrane damage (Korzeniewski and Callewaert, 1983). Table 10 shows the percentages of LDH release of the experimental conditions that were further applied in the proliferation assay.

Table 10. LDH release after treatment with indicated substances.
The maximal cytotoxicity as reference is 100,00 % (assayed according to the manufacturer's instructions). Results of one preliminary experiment.

Substance	Concentration		Incubation time		LDH release	
					Control shRNA	PGP shRNA
Bleomycin	2.5	µg/µL	17	h	18,50 %	20,73 %
H_2O_2	0.1	mM	1	h	11,43 %	19,98 %
Menadione	10	µM	45	min	7,79 %	1,68 %
	1	µM	17	h	5,05 %	9,52 %

3.1.2.3 Impact of Oxidative Stress on PGP-dependent Cellular Proliferation

In terms of proliferation the hypothesis was, that oxidative eustress should have a bigger effect on control cells as their PGP activity should be susceptible to low concentrations ROS. On the contrary, oxidative distress might have a bigger effect in terms of reducing proliferation on PGP downregulated cells. Since PGP might be involved in repair of oxidative DNA damage, DNA repair in depleted cells might be impaired. And in consequence, cellular proliferation should be more affected. The effects of treating GC1 cells with different oxidizing and reducing agents are shown in figure 13.

Shortly after stimulation of cells by EGF, PGP was oxidized (Seifried et al., 2016). EGF treatment also enhanced EGFR-related protein kinase phosphorylation and CDR formation in PGP downregulated GC1 cells (Seifried et al., 2014, Segerer et al., 2018). So, the question was whether EGF treatment would affect proliferation in control cells by inhibition of PGP by oxidation or further reduce proliferation by promoting cytoskeletal remodeling in PGP shRNA cells. Around 56.37 % of PGP shRNA cells treated with EGF incorporated EdU (difference to treated control shRNA = 3.26 %) i.e. 5.71 % more than non-treated PGP downregulated cells ($p = 0.0239$). PGP control shRNA cells showed

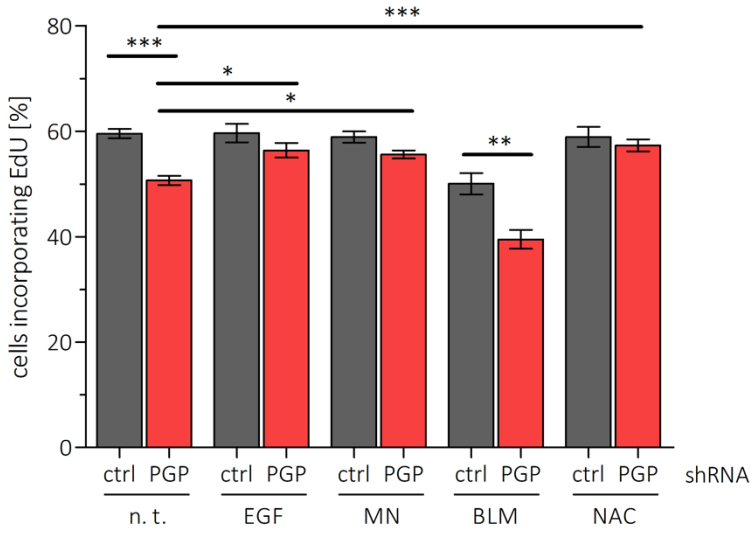

Figure 13. Impact of different oxidants and reductants on proliferation of PGP shrRNA cells compared to control shRNA cells.

*Effect of EGF (100 ng/mL, 0h), MN (1 µM, 17h), BLM (2.5 µg/mL, 17h), and NAC (10 mM, 1h) on cell proliferation. 3,000 GC1 cells per well (PGP shRNA cell line and control) were incubated with the indicated compounds (n. t. = no treatment, EGF = epidermal growth factor, MN = menadione, BLM = bleomycin, NAC = N-acetylcysteine). Proliferation was measured by quantification of the cells that incorporated EdU within 2.5 additional hours (i.e. also additional incubation time) and compared to the number of nuclei stained with Hoechst. The results represent mean values ± S.E.M. of n=3 (EGF), n=4 (MN, ctrl shRNA BLM), n=6 (NAC, PGP shRNA bleomycin), or n=18 (n. t.) independent experiments. *p<0.05; **p<0.01 ***p<0.001.*

rather no change in proliferation after EGF stimulation (59.63 %; difference to no treatment = 0.09 %). The cell culture medium is already supplied with growth factors (of fetal calf serum). Control shRNA cells might already proliferate in the highest possible rates. PGP shRNA cells on the other hand seem to be receptive for additional EGF stimulation. If PGP would be involved in feedback regulation of EGF stimulation, EGF cannot further enhance proliferation in control shRNA cells. Activation of downstream pro-proliferative enzymes and genes might be opposed to transient inactivation of PGP. When PGP is downregulated (and less active) this feedback regulation could be lacking. EGF related redox signaling probably does not cause the proliferation defect in PGP shRNA cells, but PGP seems to be important for proliferation control downstream of EGFR. It might be interesting to investigate the effect of EGF on cellular PGP activity similar to the experiments for figure 11.

MN and BLM were supposed to cause or increase oxidative DNA damage (compare detailed description above). If the proliferation defect in PGP shRNA cells could be explained by a worse handling of oxidative DNA damage, one might expect that these

cells are also more susceptible to MN or BLM treatment. Also, MN is known to directly bind to proteins or oxidize them by ROS formation which might here influence PGP activity in control cells. Since BLM does not notably induce the production of free radicals that could cause reversible thiol oxidation of enzymes, no direct PGP inhibition can be expected.

Upon overnight treatment with 1 µM MN surprisingly 55.57% of the PGP shRNA cells incorporated EdU (difference to control = 3.31 %); for non-treated cells the median was around 4.91 % lower (p = 0.0231). The proliferation of control cells might not have been affected because of the low dosage. In PGP shRNA cells MN might have induced pro-proliferative processes that were only possible because of the lacking PGP activity or counteracted by PGP-dependent processes in control cells.

BLM application was able to inhibit the proliferation of PGP shRNA cells only 1.12% more in comparison to non-treated cells (bleomycin difference = 10.54 %; p = 0.0062). DNA damage with an accumulation of 3'-PG ends, which should lead to an increase in PG release, appear to equally affect the proliferation of PGP shRNA cells and control cells. Not an increased PG content, but rather the DNA damage per se might here have an anti-proliferative effect and can most likely result from cytotoxic effects alone.

N-acetylcysteine (NAC) is the precursor of L-cysteine that physiologically mainly reduces disulfide bonds in proteins and provide thiols for the synthesis of reduced glutathione. Subordinately, it might detoxify ROS and other radicals (Samuni et al., 2013). The antioxidant is reported to reduce oxidative stress and promote proliferation in intestinal porcine epithelial cells after exogenous H_2O_2 treatment (Xiao et al., 2016). Moreover, there are several reports of pro- and anti-apoptotic as well as pro- and anti-proliferative effects of NAC by affecting redox-sensitive signaling depending on different cell types and the underlying mechanisms are too complex to be yet fully understood (Samuni et al., 2013). Besides, PGP seems to require reducing conditions (that normally prevail in the cytosol) as its activity towards PG and pNPP *in vitro* is notably increased upon addition of reductants such as DTT (figure 21) and TCEP (Seifried et al., 2016). So, NAC might promote proliferation in PGP shRNA cells if they were confronted with more endogenous oxidative stress.

NAC had rather no effect on the proliferation of control cells (remaining difference to non-treated control shRNA cells = 0.63 %). But NAC application increased proliferation in PGP downregulated cells which ended in an equalization at the level of control cells (57.31 %, difference to control shRNA cells = 1.60 %). PGP shRNA cells showed a reaction towards NAC treatment and proliferated more. It would now be interesting to assess, which pro-proliferative pathways are responsible for this reaction in GC1 cells lacking PGP activity.

H_2O_2 (0.1 mM for 1 hour) and a higher concentration of MN (10 µM for 45 minutes) had strong and comparable anti-proliferative effects both on control as well as PGP shRNA cells (EdU incorporation ranging between 31-35 %, data not shown) and thus cannot contribute to the specific investigation of PGP's role in cellular proliferation.

3.2 Inhibition of PGP Activity by Small Molecules

There is still too little knowledge about PGP itself and its biological role in detail. Previous study methods (downregulation, inactivation, knockout) might cause unknown and uncontrollable compensational reactions, that make it even harder to understand PGPs obviously complex role in physiology. Reversible oxidation as regulatory mechanism cannot be useful for experimentally modulating PGP activity because numerous other enzymes and metabolic pathways underlie redox regulation (Sies et al., 2017). So, there has been a desire for a pharmacological tool that can directly, specifically, and rapidly inhibit PGP. The focus of this work was to biochemically characterize regulating molecules as part of a major project in collaboration with other members of the research group and other institutes.

The Leibniz Institute for Molecular Pharmacology (FMP) has a stock of 41,000 compounds that meet more or less the criteria of Lipinski's Rule of Five for pharmacological applicable tools: A molecule should have no more than 5 hydrogen bond donors (nitrogen-hydrogen plus oxygen-hydrogen bonds), no more than 10 hydrogen bond acceptors (nitrogen plus oxygen atoms), a molecular mass less than 500 Da (1 Da = 1 g/mol) and an octanol-water partition coefficient log P not greater than 5 (Lipinski et al., 1997).

These small molecules were all screened against recombinant, purified PGP^{WT} using 6,8-difluoro-4-methylumbelliferyl phosphate (DiFMUP) as an artificial substrate by collaborators at the FMP. These inhibitor screens required a robust method to analyze phosphatase activity. Unfortunately, the phosphate hydrolysis from PG or PLP cannot be measured directly: special colorimetrically detectable molecules that bind to released P_i and change their absorption maximum have to be added. DiFMUP is a fluorinated molecule that can be used as artificial substrate for continuous phosphatase assays because it changes its fluorescence signal after dephosphorylation (Gee et al., 1999).

Based on a half maximal inhibitory concentration (IC_{50}) lower than 50 µM and a lack of activity against PDXP-mediated DiFMUP dephosphorylation, 37 of these compounds were tested against the physiological substrates PG (for PGP) and PLP (for PDXP as PGP's closest paralog) in a malachite green assay by Elisabeth Jeanclos. The four most promising inhibitors based on the lowest preliminary IC_{50} at (sub)micromolar

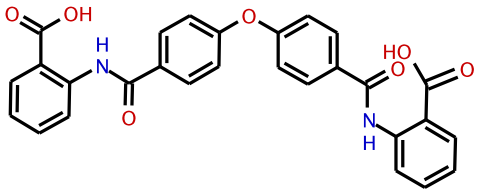

#1
2-[(4-(4-[(2-carboxyanilino)carbonyl] phenoxy)benzoyl)amino]benzoic acid
Mol. Weight 496.48 g/mol

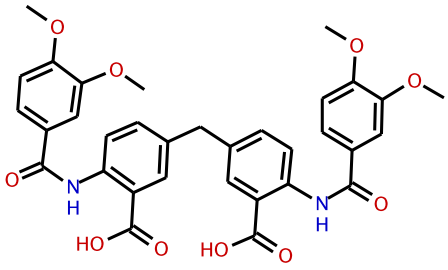

#2
5-[3-carboxy-4-[(3,4-dimethoxybenzoyl) amino]phenyl] methyl]-2-[(3,4-dimethoxy-benzoyl)amino]benzoic acid
Mol. Weight 614.61 g/mol

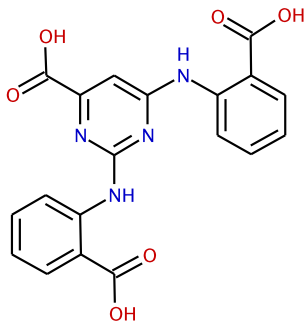

#9
2,6-bis(2-carboxyanilino)pyrimidine-4-carboxylic acid
Mol. Weight 394.35 g/mol

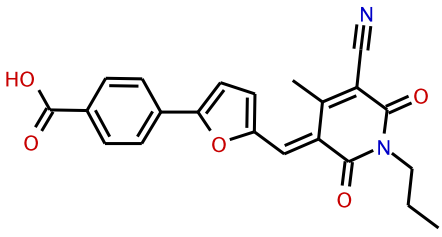

#51
4-(5-[(E)-(5-cyano-4-methyl-2,6-dioxo-1-propyl-1,6-di-hydropyridin-3(2H)-ylidene) methyl]-2-furyl)benzoic acid
Mol. Weight 390.40 g/mol

Figure 14. Chemical structures of the inhibitory compounds.
Data from Leibniz Institute for Molecular Pharmacology (FMP), ChemDiv Inc., and National Center for Biotechnology Information (PubChem Compound Database).

concentrations (from now on referred to as #1, #2, #9, and #51; see also figure 14) and chosen by Elisabeth Jeanclos were characterized in greater detail as part of this work.

3.2.1 Quantification of Inhibition

At first, the inhibitory potential towards PGP-mediated PG dephosphorylation needed to be analyzed in detail. The inhibitors were prepared in twofold serial dilutions

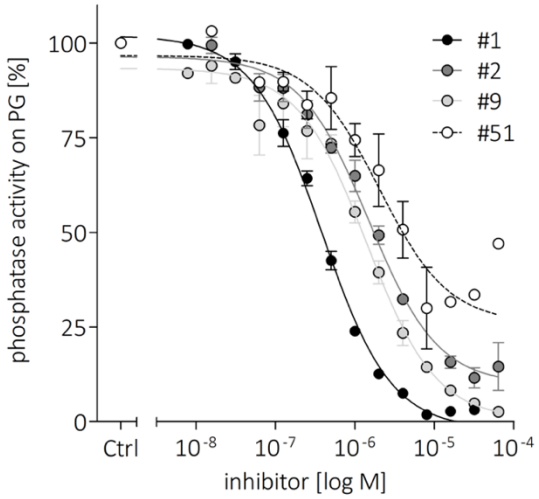

Figure 15. Concentration-response curves of the PGP-catalyzed dephosphorylation of PG in the presence of the indicated compounds.
The results represent mean values ± S.E.M. of n=3 or n=4 (#2 and #9) independently performed experiments with purified recombinant murine PGP. Error bars not seen are hidden within the symbols (#1, #2, and #9). The curve showing the effect of #51 represents only one experiment including preliminary data.

with maximal 32 µM or 64 µM respectively (based on preliminary examinations of their maximal inhibitory capacity). After incubation with highly purified, recombinant PGP (10 ng), dephosphorylation of the physiological substrate PG (200 µM) was measured.

Figure 15 shows that #1 was able to inhibit PG dephosphorylation almost completely at concentrations of 8 µM or higher. #9 reached a nearly total inhibition at 64 µM. #2 could only decrease the phosphatase activity to approximately 12 % at 32 µM. Higher concentrations resulted in an activity increase, most likely because of substrate inhibition (of the inhibiting compound).

For #51 a maximal inhibitory effect could be observed at 8 µM with about 30 % of PGP activity remaining. Beyond, the compound was light-sensitive and unstable under assay conditions and was therefore not tested further.

These graphs enabled the determination of IC_{50} values (table 12), which were micro molar or even less.

3.2.2 Inhibition of Different PGP Species and Mutants

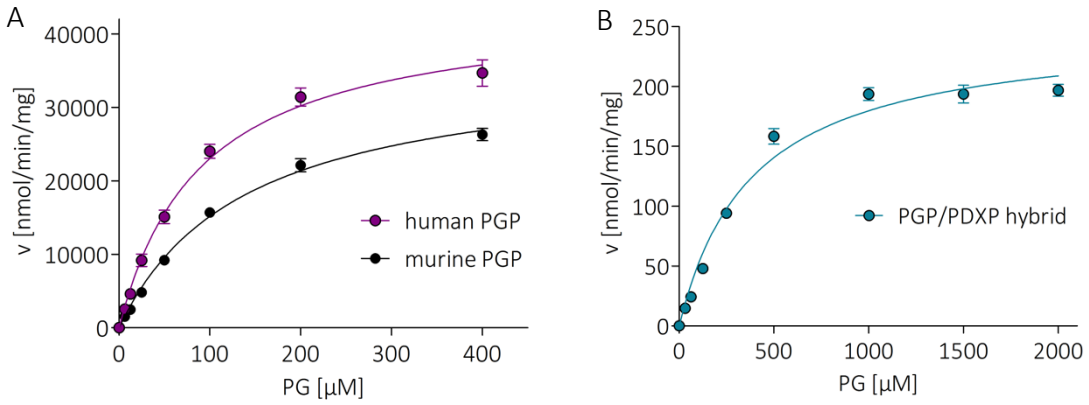

Figure 16. Steady-state kinetic measurements of murine and human PGP (A) and the PGP/PDXP hybrid (B). *Phosphoglycolate (PG) was used as substrate. Results represent mean values ± S.E.M. of n=3 independently performed experiments.*

In order to further examine the inhibitors, concentration-response measurements of PG dephosphorylation with human PGP and the PGP/PDXP hybrid were performed as well. A PGP/PDXP hybrid consisting of a PGP cap and a PDXP core was synthesized to learn more about the enzymatic structure of PGP as it was originally impossible to crystallize PGP itself (compare 1.3.1) (Seifried et al., 2014). Here, it is shown that the PGP/PDXP hybrid can dephosphorylate PG (figure 16B). The PDXP substrate PLP could neither be dephosphorylated considerably by the hybrid nor by PGP confirming the importance of the cap domain for substrate specificity (Seifried et al., 2014). To make sure that the substrate concentration was comparable, PGP/PDXP hybrid kinetics were analyzed. The used substrate concentrations should be close to K_M values and linearity of the reaction kinetics (table 11).

Table 11. Kinetic constants of PGP species and PGP/PDXP hybrid for PG and Gro3P as substrates. *The presented values for PG dephosphorylation are calculated from the data of figure 16. *The values for Gro3P dephosphorylation are taken from (Mugabo et al., 2016).*

	PG			Gro3P
	murine PGP	human PGP	PGP/PDXP hybrid	murine PGP
K_M [µM]	139	91	387	1,290*
v_{max} [nmol/min/mg]	36,198	43,892	249	175*

The curves and the IC_{50} values of the human and mouse enzymes did not differ markedly (figure 17A-D). Solely #2 showed an almost ~3-fold better inhibitory effect regarding the PG dephosphorylation by the human protein. Whereas for #9 also the

inhibition of PGP/PDXP hybrid activity was quite similar, #2 had a slightly worse effect on PGP/PDXP hybrid. The most remarkable deviation was observed for #1: the activity of the hybrid could only be inhibited to 50 % at ~17-fold higher concentrations.

In addition, it was interesting whether the compounds are also potent inhibitors for the dephosphorylation of other PGP substrates. The suppression of phosphate hydrolysis from Gro3P was tested exemplarily with compound #1 (Figure 17E). Although murine PGP activity towards Gro3P cannot be totally blocked at the highest concentrations and the IC_{50} is about ~3-fold elevated, it still remains a potent inhibitor.

The IC_{50} values are summarized in table 12.

Table 12. IC_{50} values for the PGP- or PGP/PDXP hybrid-mediated dephosphorylation PG or Gro3P in the presence of the indicated compounds.

The results represent mean values ± S.E.M. of n=3 or n=4 (#2 and #9 against PG dephosphorylation by PGP) independently performed experiments.

	IC 50 [µM] (PG)			IC 50 [µM] (Gro3P)
	murine PGP	human PGP	PGP/PDXP hybrid	murine PGP
#1	0.37 ± 0.03	0.39 ± 0.03	6.17 ± 0.63	1.05 ± 0.14
#2	1.49 ± 0.17	0.61 ± 0.07	2.51 ± 0.26	*not tested*
#9	0.86 ± 0.07	0.97 ± 0.09	0.93 ± 0.08	*not tested*
#51	2.04 ± 0.67	1.34 ± 0.31	*not tested*	*not tested*

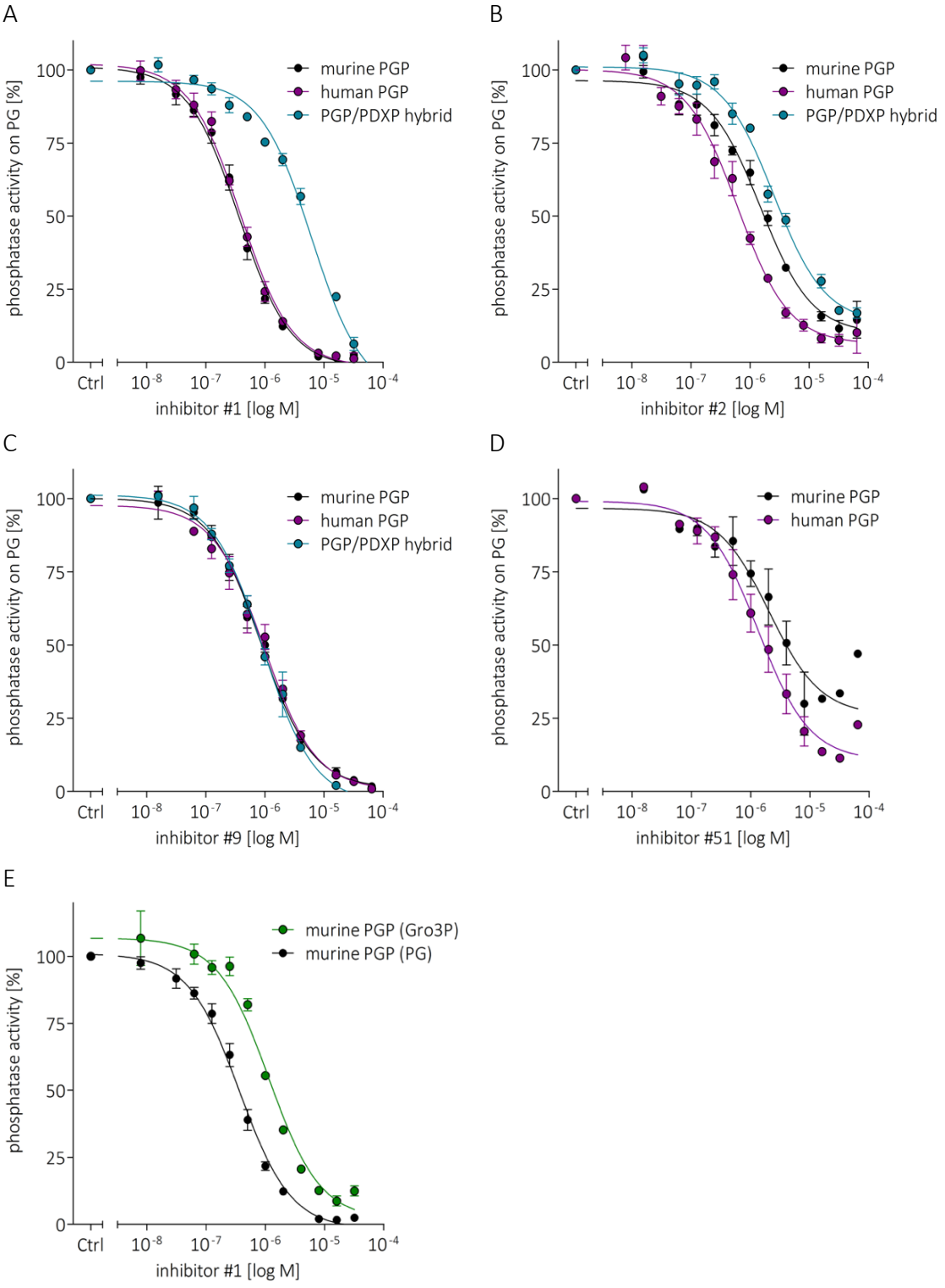

Figure 17. Concentration-response curves of the murine PGP, human PGP, or PGP/PDXP hybrid-mediated dephosphorylation of PG in the presence of the indicated compounds (A-D). Concentration-response curve of PGP-mediated PG or Gro3P dephosphorylation in the presence of compound #1 (E).

The results represent mean values ± S.E.M. of n=4 (#2 and #9) or n=3 (all others) independently performed experiments. Error bars not seen are hidden within the symbols (#1, #2 and #9). The curves showing the effect of #51 represents only one experiment.

3.2.3 Biochemical Characterization of the Inhibitors

After the quantification of PGP inhibition, the FMP compounds needed to be qualified as competitive, uncompetitive or non-competitive. For this purpose, steady-state kinetics with different substrate concentrations and different inhibitor concentrations were measured (figure 18) and the kinetic constants were calculated (table 13).

Rising concentrations of #1 lead to only a little change in K_M (maximal about 3.5-fold) compared to the other compounds, whereas v_{max} decreases up to about 2.5-fold at the highest compound concentration, suggesting that this compound performs a mix of noncompetitive and competitive inhibition. Such a mixed inhibitor might bind allosterically but a complex of enzyme, inhibitor, and substrate would still have - although reduced - remaining catalytical activity (compare 1.4.3) (Sharma, 2012).

Upon treatment with #2 and #9 v_{max} stays constant, but K_M increases up to approximately 7-fold (#2) and about 12-fold (#9), which might hint at a competitive inhibition. The higher the inhibitor concentration, the more the substrate competes for the binding site of the enzyme.

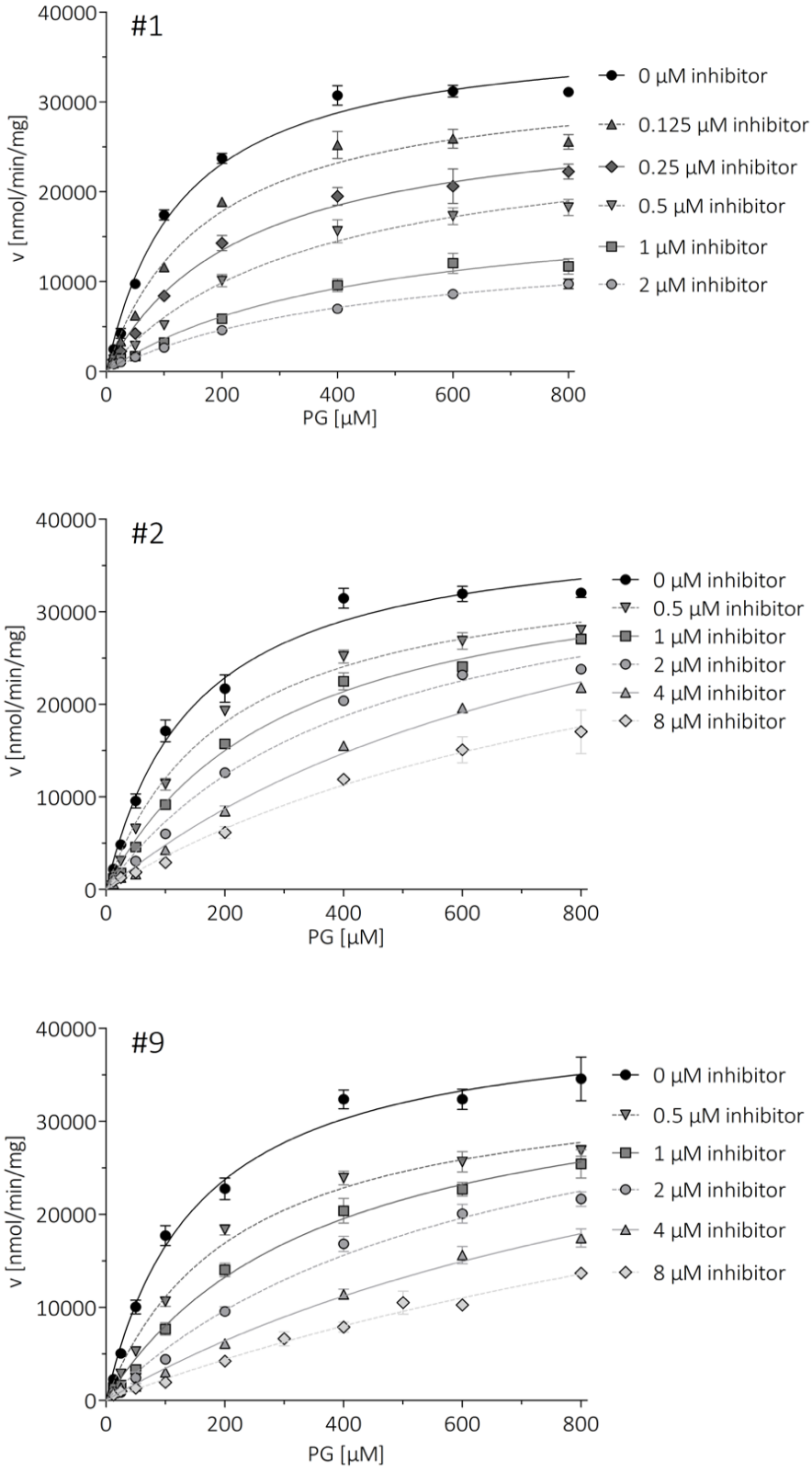

Figure 18. Kinetic measurements of PGP with inhibitors.
The results represent mean values ± S.E.M. of n=3 independent experiments. Control measurements were performed in buffer without inhibitor.

Table 13. Kinetic constants of the PGP-catalyzed PG dephosphorylation in the presence of inhibitors #1, #2, and #9.
The presented values are calculated from the data of figure 18. k_{cat} values were calculated from v_{max} using a molecular mass of 34.541 kDa for murine PGP.

		Inhibitor concentration [µM]							
		0	0.125	0.25	0.5	1	2	4	8
#1	K_M [µM]	130 ± 11.9	174 ± 21.4	235 ± 33.7	354 ± 58.3	425 ± 93.4	452 ± 48.2		
	V_{max} [nmol/min/mg]	38,156 ± 1,077	33,299 ± 1,382	29,349 ± 1,584	27,341 ± 1,974	19,117 ± 1,976	15,131 ± 776		
	K_{cat} [s^{-1}]	21.6 ± 0.4	18.9 ± 0.8	16.6 ± 0.8	15.5 ± 0.6	10.8 ± 0.9	8.58 ± 0.5		
	K_{cat}/K_M [$s^{-1}\cdot M^{-1}$]	16.6 x 10^4	10.8 x 10^4	7.1 x 10^4	4.4 x 10^4	2.5 x 10^4	1.9 x 10^4		
#2	K_M [µM]	148 ± 16.0			201 ± 16.6	297 ± 27.4	427 ± 53.9	882 ± 107.6	1,016 ± 318.5
	V_{max} [nmol/min/mg]	39,731 ± 1,382			36,137 ± 1,065	37,250 ± 1,412	38,601 ± 2,295	47,175 ± 3,522	39,884 ± 8,168
	K_{cat} [s^{-1}]	22.5 ± 0.5			20.5 ± 0.1	21.1 ± 0.7	21.9 ± 0.9	26.7 ± 2.1	22.6 ± 5.0
	K_{cat}/K_M [$s^{-1}\cdot M^{-1}$]	15.3 x 10^4			10.2 x 10^4	7.1 x 10^4	5.1 x 10^4	3.0 x 10^4	2.2 x 10^4
#9	K_M [µM]	151 ± 17.4			217 ± 21.9	363 ± 52.5	637 ± 109.4	1,192 ± 278.6	1,847 ± 555.2
	V_{max} [nmol/min/mg]	41,644 ± 1,555			35,240 ± 1,298	37,273 ± 2,382	40,405 ± 3,797	44,639 ± 7,009	44,920 ± 10,533
	K_{cat} [s^{-1}]	23.6 ± 0.9			19.97 ± 0.5	21.13 ± 1.0	22.9 ± 0.5	25.3 ± 3.3	25.46 ± 5.5
	K_{cat}/K_M [$s^{-1}\cdot M^{-1}$]	15.7 x 10^4			9.2 x 10^4	5.8 x 10^4	3.6 x 10^4	2.1 x 10^4	1.4 x 10^4

3.2.4 Outlook - Application of the Inhibitor Molecules

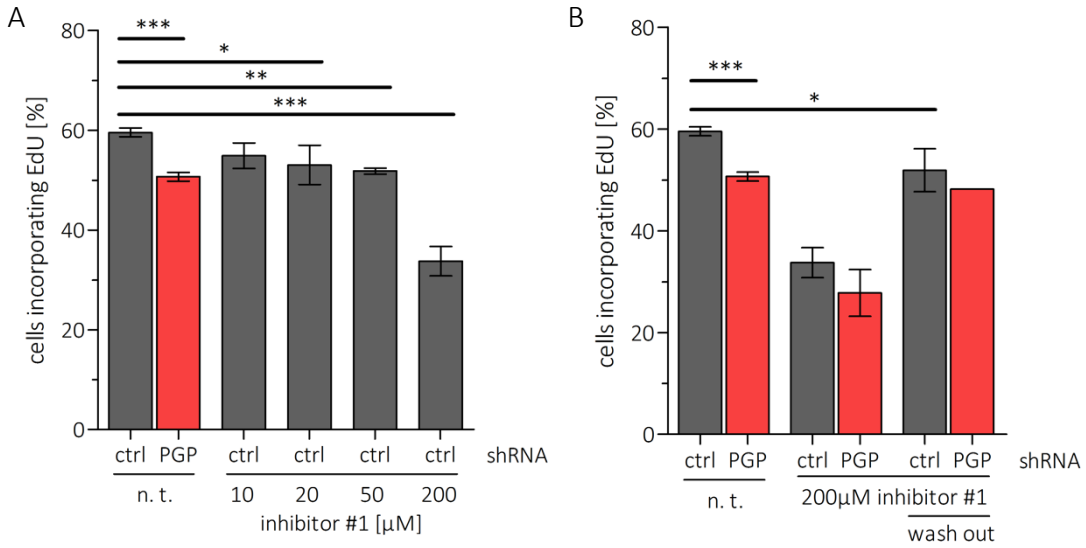

Figure 19. Application of #1 leads to a concentration-dependent and reversible reduction of cellular proliferation in GC1 cells.
*(A) Effect of inhibitor #1 in different concentrations for 1 hour on cell proliferation. (B) Cellular proliferation is normalized when the inhibitor is "washed out". For the "wash out" cells were incubated with #1 for 1 hour followed by an exchange of medium without inhibitor and incubation without special treatment for another hour. 3,000 GC1 cells per well (PGP shRNA cell line and control) were incubated with the indicated concentrations of inhibitor #1 (n. t. = no treatment). Proliferation was measured by quantification of the cells that incorporated EdU within 2.5 additional hours (i.e. also additional incubation time) and compared to the number of nuclei dyed with Hoechst. The results represent mean values ± S.E.M. of n=1 (200 µM wash out), n=2 (20 µM; PGP shRNA with #1 200 µM), n=3 (200µM wash out), n=4 (control shRNA with AUM inhibitor #1 10 µM, 50 µM & 200 µM), or n=18 (n. t.) experiments. *p<0.05; **p<0.01 ***p<0.001.*

Now, the suitability of these potent *in vitro* inhibitors had to be examined for application in cell culture. Preliminary results show a concentration-dependent decrease of cellular proliferation upon treatment with #1 for 1h before addition of EdU (figure 19A). Lower concentrations of #1 (10 µm: 54.89 %, not significant; 20 µm: 53.03 %, p = 0.0433; 50 µm: 51.81 %, p = 0.0010) approximate a proliferation defect comparable to the effect of shRNA mediated downregulation of PGP expression (50.66 %, control shRNA: 59.54 %). It can be assumed that this effect is not a result of cytotoxicity because LDH release does not correlate with increasing inhibitor concentrations (table 14). Interestingly, #1 had a slightly lower cytotoxic effect on PGP shRNA cells compared to PGP containing control cells. The proliferation defect is mostly reversible (control: 51.89 %, PGP shRNA: 48.18 %) when the compound washed out, i.e. the medium is exchanged into fresh medium without inhibitor after one hour of incubation with #1 (figure 19B). The "wash out" is supposed to dilute the inhibitor concentration (also intracellularly) and

thus reduce its anti-proliferative effect. Hence, the inhibitory effect of #1 on cellular proliferation seems reversible. However, it has to be validated whether #1 exerts these anti-proliferative effects only by intracellular PGP inhibition.

Residual PGP activity might explain why application of a high inhibitor concentration (200 µM) drastically reduces proliferation in control shRNA cells as well as in downregulated cells (control: 33.74 %, PGP shRNA: 27.80 %). Another explanation might be a yet unknown side target of #1 causing an anti-proliferative effect. Still, more research has to concentrate on the specificity and exclusiveness of PGP inhibition by #1.

Only the impact of #1 on cellular proliferation was analyzed because of its highest inhibitory potency and its particular mode of action as mixed (noncompetitive) inhibitor. However, also #2 and #9 were not too cytotoxic under the investigated treatment conditions (table 14). The different concentrations were chosen on the basis of the respective IC_{50} values. The concentrations should be high enough to reach a maximal PGP inhibition in the cells.

Table 14. LDH release after treatment with PGP inhibitors.
The maximal cytotoxicity as reference is 100,00 % (assayed according to the manufacturer's instructions). Results of one preliminary experiment.

Substance	Concentration	Incubation time	LDH release	
			Control shRNA	PGP shRNA
PGP inhibitor #1	10 µM	3 h	12,27 %	9,93 %
	50 µM	3 h	11,47 %	6,03 %
		1 h	7,57 %	1,33 %
	200 µM	1 h	7,17 %	2,17 %
PGP inhibitor #2	30 µM	3 h	13,01 %	12,50 %
	50 µM	3 h	11,51 %	5,49 %
		1 h	10,46 %	2,26 %
	200 µM	1 h	6,62 %	1,98 %
PGP inhibitor #9	20 µM	3 h	11,76 %	10,67 %
	50 µM	3 h	4,60 %	1,20 %
		1 h	8,94 %	1,41 %
	200 µM	1 h	2,92 %	2,02 %

4 Discussion

This thesis work presents progress regarding mechanisms of PGP regulation: transient inhibition of cellular PGP activity upon incubation of cells with H_2O_2 could be demonstrated for the first time, and novel pharmacological PGP inhibitors could be characterized. In addition, attempts were made to study PGP-dependent cellular responses to oxidative stress. However, the obtained results only yielded preliminary indications.

4.1 Impact of PGP Downregulation on Redox Signaling and Oxidative (DNA) Damage

Because PGP-depleted cells grow significantly more slowly, it can be suggested that proliferation depends on PGP activity (figure 12). This proliferation defect could not be related to the inability of PGP shRNA cells to cope with oxidative DNA damage. From the presented approaches the influence of reversible oxidation and transient inactivation of PGP influence proliferation can only be guessed.

4.1.1 Induction or Enhancement of Oxidative stress

The ROS-formation by MN corresponds to the mechanism of H_2O_2-mediated DNA damage. Additionally, MN itself can bind to and damage DNA as semiquinone radical (Klotz et al., 2014). MN furthermore seems to affect protein thiol oxidation via ROS formation or also direct binding (Di Monte et al., 1984). In this work, MN temporarily activated cellular PGP (figure 11B, not significant) and increased proliferation in PGP-depleted cells upon overnight treatment compared to non-treated PGP-depleted cells (figure 13). An explanation might be the treatment concentration: a remarkable increase in protein thiol oxidation was reported only for concentrations higher than 200 µM, lower concentrations only oxidize about 20 % of protein thiols (Di Monte et al., 1984) whereas considerable DNA damage occurred at concentrations beginning from 10 µM (Morrison et al., 1984). For the present work, concentrations beyond 21% of cytotoxicity (table 10)

were used, especially longtime incubation (17 h) in concentrations higher than 5 µM exceed this value. At concentrations around 40 µM MN could even stimulate pro-proliferative EGFR signaling (presumably independent of ROS formation) (Klotz et al., 2014). However, treatment of GC1 cells with 10 µM MN for only 45 minutes had already strong anti-proliferative effects that could not be related to PGP downregulation (data not shown). The very low concentration applied herein (1 µM for 45 minutes) might not have sufficed to oxidize PGP or notably damage DNA but was enough to induce pro-proliferative signaling in PGP shRNA cells (figure 13). Somehow, PGP depleted cells were responsive to pro-proliferative stimuli. This would fit with the comparable proliferation increase in PGP shRNA cells after EGF treatment. PGP was already supposed to be involved in an EGFR signaling feedback loop (Segerer et al., 2018) that might properly work in (intact) control cells. The physiological implication of PGP in EGF signaling is perhaps focused on short-term regulation. This reaction might be impaired in PGP depleted cells and prolong or intensify EGF-mediated effects.

However, it might be interesting to investigate the interaction of MN with purified PGP^{WT} in activity assays and maybe also in co-crystallization experiments as well as the impact of EGF on cellular PGP activity (according to the experiments with MN and H_2O_2 shown in figure 11).

H_2O_2 can inhibit PGP after direct application (or maybe also secondarily after EGF stimulation). A reversible short-term (a few minutes) inhibition of PGP by oxidation was first described by (Seifried et al., 2016) and could also be shown in figure 11A. This can be compared to other reports of phosphatase inhibition by thiol oxidation via H_2O_2 (Klomsiri et al., 2011). In higher concentrations H_2O_2 induces SSBs and DSBs via intracellular formation of ROS (Driessens et al., 2009). Unfortunately, it was not possible to show a divergent metabolic effect in PGP shRNA and control cells upon H_2O_2-treatment because the cytotoxicity (table 10) and PGP independent anti-proliferative effects predominated (EdU incorporation reaching around 30-35 % after treatment with 0.1 mM H_2O_2 for 1 or 17 hours, data not shown).

4.1.2 Minimized Oxidative Stress or Normalized Glycerolipid Partitioning

The antioxidant and glutathione precursor NAC can maintain redox homeostasis and thus reduce oxidative distress (Samuni et al., 2013). As oxidative stress can be associated with lipid accumulation NAC treatment (10 µM - 5 mM) could reduce ROS and TG levels (Pieralisi et al., 2016, Calzadilla et al., 2011). Moreover, NAC seems to promote proliferation independently of its antioxidant properties (Yi et al., 2016, Xiao et al., 2016). Treatment with NAC enhances proliferation in PGP-depleted cells but has no effect on control cells (figure 13). However, NAC treated cells (10 mM) were not exposed to harmful oxidants beforehand. Maybe PGP depletion (where lipid accumulation is reported) causes an oxidative stress-like situation after all which is here counteracted by NAC. Or maybe NAC just influences the altered lipid metabolism in PGP shRNA cells from TG accumulation towards proliferation what might be supported by the effect of blocking TG cycling (supplementary data, figure 23) (Segerer et al., 2018).

4.1.3 No PGP-dependent Effect of DNA Damage with 3'PG-ends in GC1 Cells

A direct increase of 3'-PG-end containing DNA damage can be induced by BLM. In *E. coli* PGP-deficient cells are significantly more affected by this kind of DNA damage making it a reasonable source of PG (Pellicer et al., 2003). In the present work, the proliferation decrease of control and PGP shRNA cells was comparable upon bleomycin treatment, the difference increased only by 1.12 % (figure 13). *Gph* (gene name of enzyme with PG phosphatase activity from *E. coli*) is phylogenetically different from human (or mammalian) PGP. Another HAD phosphatase from *E. coli*, NagD that dephosphorylates nucleotides, corresponds structurally with PGP, PDXP, and LHPP in humans and Pho13 from *S. cerevisiae* (Kuznetsova et al., 2015). While PGP depletion in mammals did not cause elevated PG levels resulting from DNA repair Pho13 depletion did cause an 8-fold increase (Collard et al., 2016). PGP activity must have developed early in evolution and its paralogs can change substrate specificity quickly remembering the HAD superfamily as biggest family that acts upon phosphorylated small metabolites (Tremblay et al., 2006, Kuznetsova et al., 2006). So, the functions of PGP and the effects

of lacking its activity can also vary in different domains, kingdoms, classes, families, and species.

4.2 Directed Control of PGP Activity

Because of the vague and hardly interpretable results of investigating PGP-dependent proliferation in the context of oxidative stress, new approaches to facilitate structural and metabolic analyses of PGP were required. A pharmacological tool to directly inhibit PGP activity should be found. The results of this work present the characterization of such a molecule. The exclusiveness and the rapidity of PGP inhibition remain to be evaluated.

4.2.1 Classification of the Identified Inhibitory Molecules

Among the tested compounds, #1 was the most potent PGP inhibitor. Probably compound #1 is a mixed inhibitor combining noncompetitive (allosteric) and competitive inhibition. Rising inhibitor concentrations induced a constant decrease in v_{max} and only a little change in K_M (in comparison to the other inhibitors, figure 18 and table 13) (Sharma, 2012, Berg et al., 2018). Compared to PGP, the PGP/PDXP hybrid was less sensitive to inhibition by #1 (figure 17A). The molecule seems to (also) bind to the core domain which differs between PGP and the hybrid (which has the PDXP core domain). Structural studies are planned to identify the binding site and mode of action of #1.

#2 and #9 are competitive PGP inhibitors. Rising compound concentrations lead to an increased K_M value, whereas v_{max} does not change markedly (figure 18 and table 13). Additionally, the inhibitory capacity did not change upon the different protein types (figures 17B and C). That means, the more inhibitor is there, the more the substrate competes for the binding site of the enzyme. v_{max} stays constant because the enzymes are only reversibly bound by inhibitors, thus they stay available for substrate conversion (Sharma, 2012, Berg et al., 2018). A competitive mode of inhibition is also considerable regarding the molecular size of the compounds. #2 as the biggest molecule (614.61 g/mol; figure 14) is only about three to four times bigger than the physiological

compounds (from 156.03 g/mol for PG to 216.08 g/mol for 4PE; figure 3); #9 (394.35 g/mol; figure 14) is even smaller. The C2a-type cap of PGP is especially selective for small substrates (Gohla, 2018, Seifried et al., 2014).

The catalytic efficiency decreases drastically in all cases.

4.2.2 Advantages and Disadvantages of Inhibitors

Inhibitors can be applied to overcome the compensatory effects that are frequently observed when e.g. the activity of an enzyme is suppressed by (RNA-interference-mediated) downregulation, by a knockout of the gene, or by a knockin replacement with an inactive enzyme mutant (as it has been the case for previous approaches to study the biological role of PGP). A reversible inhibitor furthermore allows to control the duration of enzyme inhibition because it is effective as long as its concentration is maintained at a high enough level.

Selective inhibitors of PGP have not been discovered so far. Phosphate mimics and thus phosphatase inhibitors such as orthovanadate (for PTPs) and BeF_3^- (HAD phosphatases) could also impair PGP activity (Seifried et al., 2014). Vanadium compounds are used as competitive broad-specificity inhibitors of PTPs in various experimental set-ups (Irving and Stoker, 2017). As supposed pan-inhibitor of the whole PTP superfamily (because of the highly conserved structural and sequence similarity at the active site), there might always be off-target or uncontrollable effects in cell culture, animal models, or clinical trials (Irving and Stoker, 2017). The metal fluoride BeF_3^- is mainly used as tool for structural and computational analysis (Jin et al., 2017). Both inhibitors are not highly selective for a certain enzyme but rather for a small group of enzymes (Irving and Stoker, 2017, Jin et al., 2017). To analyze the effects of blocking one particular enzymatic activity (here PGP) in cell culture (and maybe later in animal models) a selective inhibitor ideally without off-target effects is necessary.

As compound #1 already shows different inhibiting effects on PGP compared to the PGP/PDXP hybrid molecule and might therefore bind allosterically, it could be a highly specific inhibitor. Compounds #2 and #9 with competitive inhibition properties might not be comparably specific assuming that they inhibit at the active site in the core domain

whose structure is not as unique as the cap domain compared to other HAD phosphatases. However, #2 and #9 do not resemble the physiological substrates that much (compare figures 3 and 14) and might somehow match structurally especially PGP. In each case the structure of an inhibitor must fit the targeted enzyme structure. A molecule might even inhibit only one of two structurally similar enzymes because of one different residue (altering redox potential, load, or acid/base reactivity). If an exclusive effect is aimed, similar enzymes have to be counter-tested. Recent experiments showed, that the identified compounds (#1, #2, and #9) do not affect the enzymatic activity of some related HAD-type phosphatases in a comparable manner (Gohla group, unpublished results). Further experiments with resembling phosphatases are in progress.

One major difficulty for these new inhibitory molecules is their transport into the cytosol. Regarding the molecular weight of all three compounds (with 614.61 g/mol #2 is the biggest molecule), the passage of the cellular membrane seems likely (Lipinski et al., 1997). Preliminary experiments (figure 19) induced a partially reversible concentration-dependent proliferation decrease. A concentration of 50 µM of #1 was comparable to downregulation by shRNA. Ongoing experiments evaluate the suitability of #1 as an inhibitor of PGP in eukaryotic cells.

Off-target effects next to PGP inhibition also have to be examined.

4.3 Possible Applications of the Inhibitor(s)

PGP is safeguarding cellular metabolism: it degrades potentially useless or toxic metabolic side products (Collard et al., 2016), connects glucose and lipid metabolism (Mugabo et al., 2016), and acts at the intersection between triacylglyceride build-up (storage, resting state) and membrane build-up (proliferation, reproduction) (Segerer et al., 2016, Segerer et al., 2018). So, the question arises whether regulatory disorders of PGP are associated with diseases such as obesity, diabetes mellitus, and/or cancer (Gohla, 2018).

To protect itself from mutagenesis, reproduction/cell division is arrested in case of too much DNA damage (Berg et al., 2018). Since PGP seems to be important for cellular proliferation it might be a target in cancer therapy. Unfortunately, still too little is known

about the physiological role of PGP in detail and until now, there is no report of a tumor linked to PGP hyperactivity. Therapeutic inhibition thus might only be aimed when PGP activity or expression is pathologically high.

Although PGP function appears to be important for healthy cellular metabolism, no metabolic diseases have yet been discovered associated with PGP dysfunction. If so, especially a stimulation (and no inhibition) of PGP activity would be interesting. PGP overexpression in rat liver and rat pancreas gave first hints to beneficial effects of increased PGP availability in terms of reduced TG levels and glucolipotoxicity (Mugabo et al., 2016). However, constitutive overexpression is not the same as activation of an enzyme and might also change the substrate spectrum (Gohla, 2018).

As we learn from the introduction, a lot of features and functions of PGP still remain unclear. First of all, the inhibitor shall enable new research methods for understanding (the role of) this enzyme. Structural analyses can be supported by co-crystallization with the inhibitory molecules. Short- and long-term metabolic changes could be observed without the compensatory reactions of a downregulation of the gene, a knockin of inactivated protein, or a knockout.

5 Summary

Mammalian phoshoglycolate phosphatase (PGP, also known as AUM) belongs to the ubiquitous HAD superfamily of phosphatases. As several other members of HAD phosphatases, the Mg^{2+}-dependent dephosphorylation is conducted via a nucleophilic attack from a conserved aspartate residue in the catalytic cleft. The protein structure of PGP could not yet be solved entirely. Only a hybrid consisting of the PGP cap and the PDXP core (pyridoxal phosphatase, closest enzyme paralog) was crystallizable so far. PGP is able to efficiently dephosphorylate 2-phosphoglycolate, 2-phospho-L-lactate, 4-phospho-D-erythronate, and glycerol-3-phosphate *in vitro* which makes them likely physiological substrates. The first three substrates can be derived from metabolic side reactions (during glycolysis) and inhibit key enzymes in glycolysis and pentose phosphate pathway, the latter is situated at the intersection between glycolysis and lipogenesis. 2-phosphoglycolate can also be released in the context of repair of oxidative DNA damage. The activity of purified PGP can be reversibly inhibited by oxidation - physiologically likely in association with epidermal growth factor (EGF) signal transduction. In fact, an association between persistently lacking PGP activity (via downregulation) and the presence of hyperphosphorylated proteins after EGF stimulation has been identified. Reversible oxidation and transient inactivation of PGP may be particularly important for short-term and feedback regulatory mechanisms (as part of the EGF signaling). Furthermore, cellular proliferation in PGP downregulated cells is constantly reduced. Whole-body PGP inactivation in mice is embryonically lethal. Despite the many well-known features and functions, the knowledge about PGP is still incomplete.

In the present work the influence of reactive oxygen species (ROS) on PGP activity in cells und a possible connection between oxidative stress and the proliferation deficit of PGP downregulated cells was investigated. For the experiments, a spermatogonial cell line was used (due to the high PGP expression in testis). PGP activity can be reversibly inhibited in cellular lysates by H_2O_2 (as a ROS representative). Reversible oxidation could thus indeed be physiologically important. More oxidative DNA damage (by bleomycin) showed no PGP-dependent effects here. EGF stimulation (as an inducer of transient and

well-controlled ROS production), low concentrations of menadione (as an oxidant) and N-acetylcysteine (as an antioxidant) were able to approximate the proliferation rate in PGP downregulated cells to that of control cells. The redox regulation of PGP could thus have an influence on cellular proliferation as a feedback mechanism - a mechanism that could not take place in PGP downregulated cells. However, the connections are probably even more complex and cannot be elucidated by a sole examination of the proliferation rate. The present results can thus only be regarded as preliminary experiments.

For a better understanding of the features and functions of PGP, this work then focused on specific regulation of enzyme activity by pharmacologically applicable small molecules. Four potent inhibitors had previously been identified in a screening campaign. In this work, three of these four inhibiting compounds could be further characterized in experiments with highly purified, recombinant murine and human PGP. Compounds #2 and #9 showed competitive inhibition properties with a markedly rising K_M value with little or no change in v_{max}. The results were consistent for all tested protein variants: the murine and the human PGP as well as a PGP/PDXP hybrid protein. Compound #1 was the most potent and interesting PGP-inhibitory molecule: less change in K_M and a constant decrease in v_{max} as well as a lower impact on the PGP/PDXP hybrid hint at a mixed mode of inhibition as a combination of competitive and non-competitive inhibition. The characterization of the potential inhibitors can serve as a basis for further structural analysis and studies on the complex physiological role of PGP.

Zusammenfassung

Die Phosphoglykolat-Phosphatase (PGP, auch AUM genannt) in Säugetieren gehört zu der ubiquitär vorkommenden HAD Phosphatasen-Superfamilie. PGPs Proteinstruktur konnte bisher nicht vollständig gelöst werden. Es ließ sich nur ein Hybridenzym, bestehend aus der PGP-Kappe und dem PDXP-Kern (Pyridoxal-Phosphatase, am nächsten verwandtes Enzym), kristallisieren. Wie zahlreiche andere Mitglieder der HAD Phosphatasen, geschieht die Magnesium-abhängige Dephosphorylierung durch eine nukleophile Attacke eines konservierten Aspartat-Rests im katalytischen Zentrum. PGP ist in der Lage 2-Phosphoglykolat, 4-Phospho-D-Erythronat, 2-Phospho-L-Laktat und Glycerol-3-Phosphat *in vitro* zu dephosphorylieren, was sie zu wahrscheinlichen physiologischen Substraten macht. Die ersten drei Substrate können durch metabolische Nebenreaktionen (während der Glykolyse) entstehen und Schlüsselenzyme in Glykolyse und Pentosephosphatweg inhibieren, das letztgenannte findet sich an der Kreuzung zwischen Glykolyse und Lipogenese. 2-Phosphoglykolat kann auch im Rahmen der Reparatur von oxidativem DNA-Schaden freigesetzt werden. Die Aktivität von gereinigtem PGP kann durch Oxidation - physiologisch wahrscheinlich assoziiert mit der Signaltransduktion des epidermalen Wachstumsfaktors (EGF) - reversibel inhibiert werden. Es wurde nämlich auch ein Zusammenhang zwischen dauerhaft mangelnder PGP-Aktivität (durch Herabregulation) und dem Vorkommen hyperphosphorylierter Proteine nach EGF-Stimulation festgestellt. Reversible Oxidation und vorübergehende Inaktivierung der PGP könnten vor allem für Kurzzeit- und Rückkopplungs-Regulationsmechanismen (im Rahmen der EGF-Signalkaskade) bedeutend sein. Weiterhin ist die zelluläre Proliferation in PGP-herabregulierten Zellen konstant reduziert. Eine PGP-Inaktivierung im gesamten Organismus in Mäusen ist embryonal letal. Trotz der vielen inzwischen bekannten Eigenschaften und Funktionen ist das gesammelte Wissen über PGP noch lückenhaft.

In der vorliegenden Arbeit wurde zunächst der Einfluss von reaktiven Sauerstoffspezies (ROS) auf die PGP-Aktivität in Zellen und ein möglicher Zusammenhang zwischen oxidativem Stress und dem Proliferationsdefizit von PGP-herabregulierten

Zellen untersucht. Für die Experimente wurde (aufgrund der hohen PGP-Expression in Hoden) eine spermatogoniale Zelllinie verwendet. PGP-Aktivität kann in zellulären Lysaten reversibel durch H_2O_2 (als ROS Vertreter) gehemmt werden. Reversible Oxidation könnte also tatsächlich auch physiologisch von Bedeutung sein. Mehr oxidativer DNA Schaden (durch Bleomycin) zeigte hier keine PGP-abhängigen Effekte. EGF-Stimulation (als Auslöser von transienter und gut kontrollierter ROS-Produktion), niedrigdosiertes Menadion (als Oxidans) und N-Acetylcystein (als Antioxidans) konnten die Proliferationsrate in PGP-herabregulierten Zellen an die von Kontrollzellen annähern. Die Redox-Regulation von PGP könnte als Feedback-Mechanismus also auch Einfluss auf die zelluläre Proliferation haben - ein Mechanismus, der bei PGP herabregulierten Zellen so nicht stattfinden könnte. Wahrscheinlich sind die Zusammenhänge aber noch komplexer und mit einer alleinigen Untersuchung der Proliferationsrate nicht aufzuklären. Die vorliegenden Ergebnisse können also nur als Pionierversuche betrachtet werden.

Um die Merkmale und Funktionen von PGP besser zu verstehen, fokussierte sich die weitere Arbeit auf die spezifische Regulation der Enzymaktivität durch pharmakologisch anwendbare kleine Moleküle. Vier potentielle Inhibitoren waren zuvor in einer Screening-Kampagne identifiziert worden. In dieser Arbeit konnten drei von vier der inhibierenden Moleküle in Experimenten mit hoch-aufgereinigtem, rekombinantem murinem und humanem PGP näher charakterisiert werden. Die Moleküle #2 und #9 zeigten kompetitiv hemmende Eigenschaften mit deutlich steigendem K_M-Wert bei geringer oder gar keiner Veränderung der Maximalgeschwindigkeit (v_{max}). Die Ergebnisse waren bei allen untersuchten Protein-Varianten - murinem und humanem PGP sowie einem PGP/PDXP-Hybrid-Protein - vergleichbar. Molekül #1 war der potenteste und interessanteste PGP-Inhibitor: eine geringere Veränderung des K_M-Werts und eine konstante Verminderung von v_{max} sowie ein reduzierter Einfluss auf den PGP/PDXP-Hybriden weisen auf einen gemischten Inhibitionsmechanismus als Kombination aus kompetitiver und nicht-kompetitiver Hemmung hin. Die Charakterisierung der potentiellen Inhibitoren kann als Basis für weiterführende strukturelle Analysen und der Untersuchung der komplexen physiologischen Rolle von PGP dienen.

6 Supplementary Data

6.1 Gro3P Phosphatase Activity in GC1 Cells

It has been shown, that PGP hydrolyzes Gro3P - as purified protein *in vitro* and from lysates of 293T cells (transformed human embryonic kidney cells) and INS832/13 cells (rat pancreatic ß-cells) (Mugabo et al., 2016). Because of working with GC1 cells their lysates were tested here for an activity towards Gro3P.

The lysates of GC1 cells were prepared similar to the description above (see 2.2.5.1.2). However, the cells were lysed in only 200 µL of TMN lysis buffer in order to reach a higher concentration. After centrifugation of only 10 minutes the supernatant was transferred to 10 K filter reaction tubes (which were prerinsed with 200 µL TMN assay buffer and centrifuged with the lysates). These filter reaction tubes were again centrifuged at 4°C and 15,000 rpm for 3 minutes. The remaining supernatant was filled up to 200 µL with TMN assay buffer and centrifuged for another 4 minutes. The lysate was again filled up to 200 µL, mixed by gentle tapping and transferred into fresh Eppendorf reaction tubes.

For the assay, the buffer mix was prepared as described in table 15 and distributed on a 96 well plate, then the lysate was added. Gro3P as substrate was used in a final concentration of 0.75 mM. The following procedure was similar to the assay description in general (see 2.2.5.2) except for the inhibitor preparation.

Table 15. Composition of buffer mix with lysate for detecting Gro3P dephosphorylation by GC1 cell lysates. *DTT (dithiothreitol) as activator, TMN (TEA/triethanolamine, $MgCl_2$ and NaCl) as reaction buffer. 44 µL total volume of lysates + buffer mix.*

	Compound	per well
Lysates (e.g. control & PGP shRNA)	Lysate	10 µL
Buffer mix	TMN	33 µL
	DTT 1 M	0.5 µL
	$MgCl_2$ 250 mM	0.5 µL

Although the S.E.M. of the activity curves appear quite high, the graph shows a tendentially lower P_i release in lysates from PGP shRNA cells (figure 20). Measurement difficulties can be explained by the lower affinity of PGP towards Gro3P and more disturbing phosphate containing background in the cell lysates. Hence, PGP activity towards Gro3P seems to be present in GC1 cells.

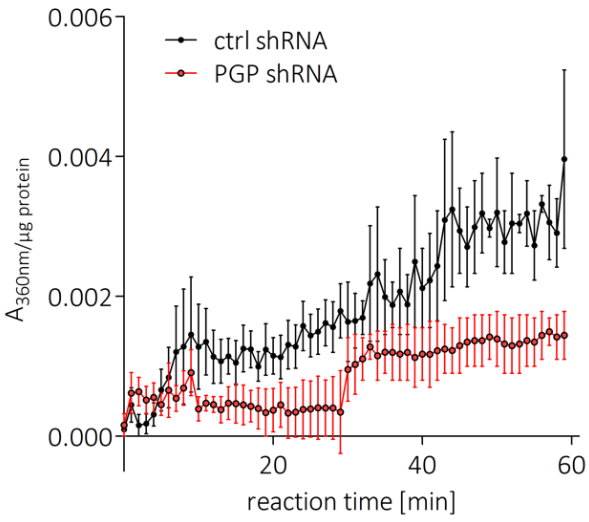

Figure 20. Cellular PGP activity in down-regulated cells compared to control cells.
PGP activity assay in GC1 cell lysates. Free phosphate released from exogenous Gro3P was measured using the EnzChek Phosphate Assay Kit. The results represent mean values ± S.E.M. of n=6 (0-29 min) or n=3 (30-59 min) independent experiments. Error bars not seen are hidden within the symbols.

6.2 Reduction-sensitivity of PGP and PDXP

Further experiments on the effect of reduction on the enzymatic activity of PGP and PDXP mainly served to improve the methods and are briefly presented here. PGP is abundant in the cellular cytosol where normally reduced conditions prevail (Berg et al., 2018). Dithiothreitol (DTT) was used as reductant that mimics dithiol containing enzymes involved in the repair of oxidized proteins (Parsons and Gates, 2013) to simulate physiological conditions. DTT has already successfully (re)activated PGP activity (Seifried et al., 2016).

6.2.1 Effect of Reduction on the Activity of Purified PGP towards PG

The PGP catalyzed dephosphorylation of the artificial substrate pNPP is enhanced by the addition of the reducing agent DTT (Seifried et al., 2016). For deeper insights into the catalytic mechanism of PGP, the redox sensitivity of PGP activity towards the physiological substrate PG was tested.

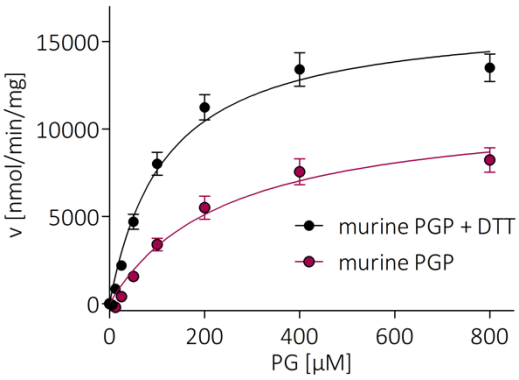

Figure 21. PGP activity increase towards PG by addition of reducing compound DTT.
Results are Mean ± SEM of n=3 (murine PGP) or n=4 (murine PGP + DTT) independent experiments.

Steady-state kinetics were measured after incubating recombinant, purified PGP^{WT} with 4 mM DTT. A control was performed without DTT. The K_M of PG dephosphorylation (245.1 µM without DTT, 116.2 µM with DTT) can be halved by the addition of DTT, whereas the v_{max} (11,344 nmol/min/mg without DTT, 16,523 nmol/min/mg with DTT) rises significantly. The values were calculated from figure 21. DTT can thus be used to improve assay conditions of PGP mediated PG dephosphorylation.

6.2.2 Effect of Reduction on the Activity of Purified PGP and PDXP towards DiFMUP

It was now interesting to see whether PGP reduction is always accompanied by an increase in activity. For the huge number of compounds whose influence on PGP activity should be investigated at the FMP, the malachite green assay was too complicated. 6,8-difluoro-4-methylumbelliferyl phosphate (DiFMUP), that changes its fluorescence signal after dephosphorylation, can be used as artificial substrate for continuous phosphatase assays at physiological or acid pH because of its low pK_a (Gee et al., 1999).

For preliminary improvement of the DiFMUP assay the sensitivity of PGP and PDXP on DiFMUP dephosphorylation under reducing conditions (i.e. the addition of DTT) were tested. TMN with 0.01 % Triton was used as buffer. DTT (1 mM) was only added to one half of the required amount of buffer. Highly concentrated recombinant murine PGP^{WT} or $PDXP^{WT}$ were diluted in TMN with 0.01 % Triton (either with or without DTT) to receive 0.5 µg per well and incubated at room temperature for 15 minutes. Meanwhile different substrate concentrations reaching from 200 to 6.25 µM (for PGP) and 50 to 3.125 µM (for PDXP) per well in a final volume of 100 µL were set up in a serial dilution. The

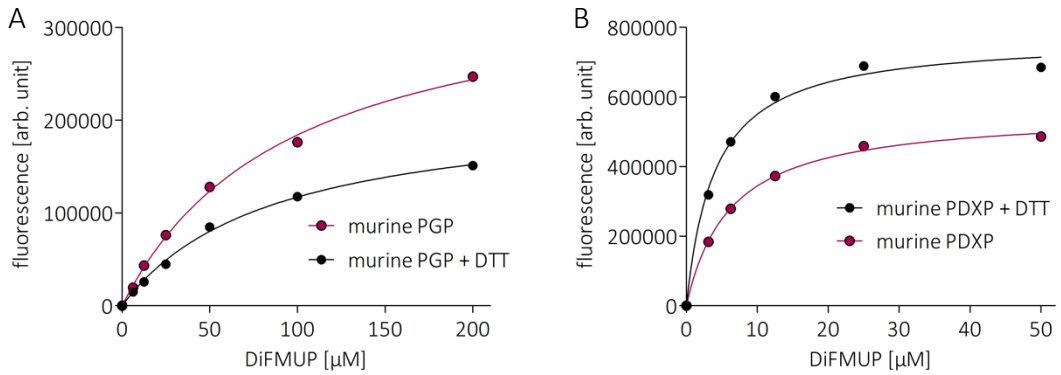

Figure 22. PGP dephosphorylation activity decrease (A) and PDXP activity increase (B) towards DiFMUP by addition of reducing compound DTT.
Compared to the respective murine protein activity without DTT. Results of only one preliminary experiment.

substrate dilutions were distributed on a 96 well plate (50 µL per well). Then pure buffer (with or without DTT) for the control or the equivalent enzyme dilutions (50 µL per well) were added as start of reaction. The fluorescence (excitation 340 nm, emission 485 nm) was recorded immediately every minute for 60 minutes at room temperature in the Envision Reader (Perkin Elmer). For kinetic measurements a time point was chosen, when the reaction was still within linearity. This assay was only performed once as preliminary experiment.

Interestingly, reduction did reduce the K_M of PGP activity as expected but also the v_{max} (figure 22A). These effects are features of uncompetitive inhibition where the "inhibitor" only binds to the enzyme-substrate-complex and then inhibits substrate conversion due to a distortion of the enzyme (compare 1.4.3) (Sharma, 2012). The catalytically important aspartate is not sensitive to redox regulation but PGP conformation indeed slightly differs when either oxidized or reduced which might explain the altered enzymatic behavior here (Seifried et al., 2016). Reduced PDXP instead lead to the expected increased DiFMUP-dephosphorylation (figure 22B). So, it might be of interest to further investigate redox regulation of PDXP. It can be concluded that regulatory mechanisms also depend on the respective substrate.

Table 16. Kinetic constants of PGP and PDXP for DiFMUP as substrate with or without DTT.
The presented values for DiFMUP dephosphorylation are calculated from the results of figure 22.

	murine PGP		murine PDXP	
	with DTT	without DTT	with DTT	without DTT
K_M [µM]	85.46	95.93	4.03	6.18
fluorescence/v_{max} [arb. unit]	217,209	360,567	771,890	556,756

6.3 Link Between Altered Lipid Metabolism and Proliferation

Previous data showed that PGP-depleted cells accumulate TGs (Segerer et al., 2016, Mugabo et al., 2016). A blockade within lipid metabolism by a combination of atglistatin and etomoxir normalized CDR formation after EGF stimulation in PGP shRNA cells (Segerer et al., 2018). Atglistatin is an inhibitor of adipose triglyceride lipase (ATGL) (Mayer et al., 2013) which hydrolyzes TGs forming diacylgylcerides (DG) (Berg et al., 2018). Etomoxir inhibits carnitine palmitoyltransferase-1 (Lopaschuk et al., 1988) that is responsible for the transfer of long-chain fatty acids into mitochondria (Berg et al., 2018). Moreover, DGAT2 (diglyceride acyltransferase 2) mRNA expression was strongly elevated in PGP inactivated murine embryos whereas DGAT1 expression remained unchanged (Segerer et al., 2016). DGAT1 and DGAT2 esterify a fatty acyid (activated by coenzyme A) to a DG as the final step of TG formation. Both enzymes are broadly expressed in mammalian tissues, albeit DGAT2 seems to dominantly contribute to TG homeostasis *in vivo* (Yen et al., 2008). A selective DGAT2 inhibitor has recently been identified (Futatsugi et al., 2015).

Compare figures 13 and 19 and 2.2.3.2 for more details on the execution of the assay. The treatment conditions for the intervention in lipid metabolism are specified in table 17.

Table 17. Concentrations of inhibitors with their incubation times before addition of EdU (implying prolonged incubation for 2.5h).

Substance	Supplier	Concentration	Incubation time
Atglistatin*	Sigma Aldrich	40 µM	1 h
Etomoxir*	Sigma Aldrich	50 µM	1 h
DGAT2 inhibitor (PF 06424439)	Tocris	1 µM	3 h

** Atglistatin and etomoxir were added together.*

Proliferation of PGP downregulated cells increased and nearly normalized upon the blockade of either TG degradation and transport into mitochondria for ATP production by atglistatin and etomoxir (difference to non-treated PGP shRNA cells = 5.31 %; p = 0.0133) or TG buildup by DGAT2 inhibitor (difference to non-treated PGP shRNA cells = 5.27 %; p = 0.0362) (figure 23). Note, that proliferation in control shRNA cells slightly decreases after incubation with the inhibitors. It can be assumed that these treatments

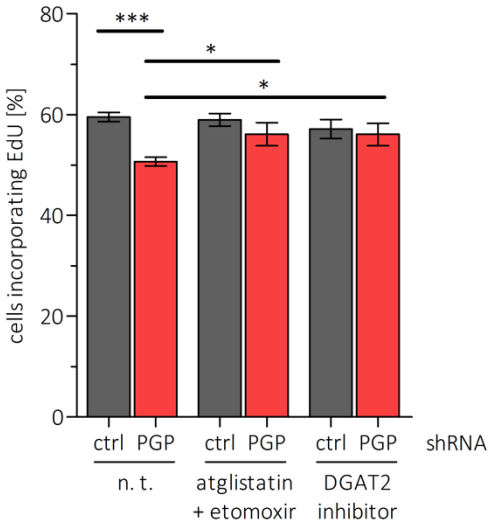

Figure 23. Inhibition of triacylglyceride (TG) build up or the use of fatty acids for ATP production promotes use of free fatty acids for membrane build up in PGP shRNA cells.

*Effect of atglistatin combined with etomoxir and DGAT inhibitor on cell proliferation (n. t. = no treatment, DGAT = diglyceride acyltransferase). Compare figures 13 and 19 and 2.2.3.2 for more details on the execution of the assay. The results represent mean values ± S.E.M. of n=3 (DGAT2 inhibitor), n=11 (atglistatin + etomoxir), or n=18 (n. t.) independent experiments. *p<0.05; ***p<0.001.*

provide for more free fatty acids in PGP depleted cells that can be used for membrane buildup rather than for cytoskeletal remodeling, storage, or energy production. PGP function thus seems important for normal physiological lipid metabolism and proliferation. Nonetheless, these experiments can only be regarded as preliminary attempts to gain further insights into the PGP related connection between lipid metabolism and proliferation and additional research is desirable.

7 References and Indices

7.1 Literature

AGUS, S. E., COX, R. P. & GRIFFIN, M. J. 1966. Inhibition of Alkaline Phosphatase by Cysteine and its Analogues. *Biochim Biophys Acta,* 118**,** 365-370.

ALLEN, K. N. & DUNAWAY-MARIANO, D. 2009. Markers of fitness in a successful enzyme superfamily. *Curr Opin Struct Biol,* 19**,** 658-65.

ANDERSON, L. E. 1971. Chloroplast and Cytoplasmic Enzymes. II. Pea Leaf Triose Phosphate Isomerases. *Biochim Biophys Acta,* 235**,** 237-244.

BERG, J. M., TYMOCZKO, J. L., GATTO JR., G. J. & STRYER, L. 2018. *Stryer Biochemie*, Springer Spektrum.

BREEN, A. P. & MURPHY, J. A. 1995. Reactions of Oxyl Radicals with DNA. *Free Radic Biol Med,* 18**,** 1033-1077.

BURDON, R. H. 1995. Superoxide and hydrogen peroxide in relation to mammalian cell proliferation. *Free Radical Biology and Medicine,* 18**,** 775-794.

BURROUGHS, A. M., ALLEN, K. N., DUNAWAY-MARIANO, D. & ARAVIND, L. 2006. Evolutionary genomics of the HAD superfamily: understanding the structural adaptations and catalytic diversity in a superfamily of phosphoesterases and allied enzymes. *J Mol Biol,* 361**,** 1003-34.

CALZADILLA, P., SAPOCHNIK, D., COSENTINO, S., DIZ, V., DICELIO, L., CALVO, J. C. & GUERRA, L. N. 2011. N-Acetylcysteine Reduces Markers of Differentiation in 3T3-L1 Adipocytes. *International Journal of Molecular Sciences,* 12**,** 6936-6951.

CHENG, Y.-C. & PRUSOFF, W. H. 1973. Relationship between the Inhibition Constant (KI) and the Concentration of Inhibitor which Causes 50 per Cent Inhibition (IC50) of Enzymatic Reaction. *Biochemical Pharmacology,* 22**,** 3099-3108.

CHO, H., WANG, W., KIM, R., YOKOTA, H., DAMO, S., KIM, S.-H., WEMMER, D., KUSTU, S. & YAN, D. 2001. Be(F3)- acts as a phosphate analog in proteins phosphorylated on aspartate: Structure of a Be(F3)- complex with phosphoserine phoshatase. *PNAS,* 98**,** 8525-8530.

COHEN, P. 2001. The role of protein phosphorylation in human health and disease. *FEBS J***,** 5001-5010.

COLLARD, F., BALDIN, F., GERIN, I., BOLSEE, J., NOEL, G., GRAFF, J., VEIGA-DA-CUNHA, M., STROOBANT, V., VERTOMMEN, D., HOUDDANE, A., RIDER, M. H., LINSTER, C. L., VAN SCHAFTINGEN, E. & BOMMER, G. T. 2016. A conserved phosphatase destroys toxic glycolytic side products in mammals and yeast. *Nat Chem Biol,* 12**,** 601-7.

DEWANG, P. M., HSU, N.-M., PENG, S.-Z. & LI, W.-R. 2005. Protein Tyrosine Phosphatases and their Inhibitors. *Current Medicinal Chemistry,* 12**,** 1-22.

DI MONTE, D., BELLOMO, G., THOR, H., NICOTERA, P. & ORRENIUS, S. 1984. Menadione-Induced Cytotoxicity Is Associated with Protein Thiol Oxidation and Alteration in Intracellular Ca2+ Homeostasis. *Archives of Biochemistry and Biophysics,* 235**,** 343-350.

DRIESSENS, N., VERSTEYHE, S., GHADDHAB, C., BURNIAT, A., DE DEKEN, X., VAN SANDE, J., DUMONT, J. E., MIOT, F. & CORVILAIN, B. 2009. Hydrogen peroxide induces DNA single- and double-strand breaks in thyroid cells and is therefore a potential mutagen for this organ. *Endocrine Related Cancer,* 16**,** 845-856.

FONTANILLO, M. & KOHN, M. 2016. Phosphatases: Their Roles in Cancer and Their Chemical Modulators. *Adv Exp Med Biol,* 917**,** 209-40.

FRANKENBACH, T. 2017. *Characterization of new Inhibitors of Haloacid Dehalogenase-Type Phosphatases: Kinetic analyses and cellular effects.* Bachelor of Science (B.Sc.) Bachelor Thesis, University of Würzburg, Germany.

FUHS, S. R. & HUNTER, T. 2017. pHisphorylation: the emergence of histidine phosphorylation as a reversible regulatory modification. *Curr Opin Cell Biol,* 45**,** 8-16.

FUJII, S. & BEUTLER, E. 1985. Glycolate Kinase Activity in Human Red Cells. *Blood,* 65**,** 480-483.

FUNG, H. & DEMPLE, B. 2011. Distinct roles of Ape1 protein in the repair of DNA damage induced by ionizing radiation or bleomycin. *J Biol Chem,* 286**,** 4968-77.

FUTATSUGI, K., KUNG, D. W., ORR, S. T., CABRAL, S., HEPWORTH, D., ASPNES, G., BADER, S., BIAN, J., BOEHM, M., CARPINO, P. A., COFFEY, S. B., DOWLING, M. S., HERR, M., JIAO, W., LAVERGNE, S. Y., LI, Q., CLARK, R. W., ERION, D. M., KOU, K., LEE, K., PABST, B. A., PEREZ, S. M., PURKAL, J., JORGENSEN, C. C., GOOSEN, T. C., GOSSET, J. R., NIOSI, M., PETTERSEN, J. C., PFEFFERKORN, J. A., AHN, K. & GOODWIN, B. 2015. Discovery and Optimization of Imidazopyridine-Based Inhibitors of Diacylglycerol Acyltransferase 2 (DGAT2). *J Med Chem,* 58**,** 7173-85.

GEE, K. R., SUN, W.-C., BHALGAT, M. K., UPSON, R. H., KLAUBERT, D. H., LATHAM, K. A. & HAUGLAND, R. P. 1999. Fluorogenic Substrates Based on Fluorinated Umbelliferones for Continuous Assays of Phosphatases and ß-Galactosidases. *Anal Biochem,* 273**,** 41-48.

GERIN, I., BURY, M., BALDIN, F., GRAFF, J., VAN SCHAFTINGEN, E. & BOMMER, G. T. 2019. Phosphoglycolate has profound metabolic effects but most likely no role in a metabolic DNA response in cancer cell lines. *Biochem J,* 476**,** 629-643.

GOHLA, A. 2018. Do metabolic HAD phosphatases moonlight as protein phosphatases? *Biochim Biophys Acta*.

GOHLA, A., BIRKENFELD, J. & BOKOCH, G. M. 2005. Chronophin, a novel HAD-type serine protein phosphatase, regulates cofilin-dependent actin dynamics. *Nat Cell Biol,* 7**,** 21-9.

HEPPNER, D. E. & VAN DER VLIET, A. 2016. Redox-dependent regulation of epidermal growth factor receptor signaling. *Redox Biol,* 8**,** 24-7.

HINDUPUR, S. K., COLOMBI, M., FUHS, S. R., MATTER, M. S., GURI, Y., ADAM, K., CORNU, M., PISCUOGLIO, S., NG, C. K. Y., BETZ, C., LIKO, D., QUAGLIATA, L., MOES, S., JENOE, P., TERRACCIANO, L. M., HEIM, M. H., HUNTER, T. & HALL, M. N. 2018. The protein histidine phosphatase LHPP is a tumour suppressor. *Nature,* 555**,** 678-682.

HOON, J. L., WONG, W. K. & KOH, C. G. 2012. Functions and regulation of circular dorsal ruffles. *Mol Cell Biol,* 32**,** 4246-57.

HUMPHREY, S. J., JAMES, D. E. & MANN, M. 2015. Protein Phosphorylation: A Major Switch Mechanism for Metabolic Regulation. *Trends Endocrinol Metab,* 26**,** 676-687.

IRVING, E. & STOKER, A. W. 2017. Vanadium Compounds as PTP Inhibitors. *Molecules,* 22.

ITAYA, K. & UI, M. 1966. A New Micromethod for the Colorimetric Determination of Inorganic Phosphate. *Clin Chim Acta,* 14**,** 361-366.

IYAMA, T. & WILSON, D. M., 3RD 2013. DNA repair mechanisms in dividing and non-dividing cells. *DNA Repair (Amst),* 12**,** 620-36.

JANG, Y. M., KIM, D. W., KANG, T. C., WON, M. H., BAEK, N. I., MOON, B. J., CHOI, S. Y. & KWON, O. S. 2003. Human pyridoxal phosphatase. Molecular cloning, functional expression, and tissue distribution. *J Biol Chem,* 278**,** 50040-6.

JEANCLOS, E., ALBERSEN, M., RAMOS, R. J. J., RAAB, A., WILHELM, C., HOMMERS, L., LESCH, K. P., VERHOEVEN-DUIF, N. M. & GOHLA, A. 2019. Improved cognition, mild anxiety-like behavior and decreased motor performance in pyridoxal phosphatase-deficient mice. *Biochim Biophys Acta Mol Basis Dis,* 1865**,** 193-205.

JIN, Y., RICHARDS, N. G., WALTHO, J. P. & BLACKBURN, G. M. 2017. Metal Fluorides as Analogues for Studies on Phosphoryl Transfer Enzymes. *Angew Chem Int Ed Engl,* 56**,** 4110-4128.

KAYNE, F. J. 1974. Pyruvate Kinase Catalyzed Phosphorylation of Glycolate. *Biochem. Biophys. Res. Commun.,* 59**,** 8-13.

KESTLER, C., KNOBLOCH, G., TESSMER, I., JEANCLOS, E., SCHINDELIN, H. & GOHLA, A. 2014. Chronophin dimerization is required for proper positioning of its substrate specificity loop. *J Biol Chem,* 289**,** 3094-103.

KLOMSIRI, C., KARPLUS, P. A. & POOLE, L. B. 2011. Cysteine-Based Redox Switches in Enzymes. *Antioxid. & Redox Signal.,* 14**,** 1065-1077.

KLOTZ, L.-O., HOU, X. & JACOB, C. 2014. 1,4-Naphthoquinones: From Oxidative Damage to Cellular and Inter-Cellular Signaling. *Molecules,* 19**,** 14902-14918.

KOONIN, E. V. & TATUSOV, R. L. 1994. Computer Analysis of Bacterial Haloacid Dehalogenases Defines a Large Superfamily of Hydrolases with Diverse Specifity. *J Mol Biol,* 244**,** 125-132.

KORZENIEWSKI, C. & CALLEWAERT, D. M. 1983. An Enzyme-Release Assay for Natural Cytotoxicity. *Journal of Immunological Methods,* 64**,** 313-320.

KRISHNAN, N., JEONG, D. G., JUNG, S. K., RYU, S. E., XIAO, A., ALLIS, C. D., KIM, S. J. & TONKS, N. K. 2009. Dephosphorylation of the C-terminal tyrosyl residue of the DNA damage-related histone H2A.X is mediated by the protein phosphatase eyes absent. *J Biol Chem,* 284**,** 16066-70.

KUZNETSOVA, E., NOCEK, B., BROWN, G., MAKAROVA, K. S., FLICK, R., WOLF, Y. I., KHUSNUTDINOVA, A., EVDOKIMOVA, E., JIN, K., TAN, K., HANSON, A. D., HASNAIN, G., ZALLOT, R., DE CRÉCY-LAGARD, V., BABU, M., SAVCHENKO, A., JOACHIMIAK, A., EDWARDS, A. M., KOONIN, E. V. & YAKUNIN, A. F. 2015. Functional Diversity of Haloacid Dehalogenase Superfamily Phosphatases fromSaccharomyces cerevisiae. *Journal of Biological Chemistry,* 290**,** 18678-18698.

KUZNETSOVA, E., PROUDFOOT, M., GONZALEZ, C. F., BROWN, G., OMELCHENKO, M. V., BOROZAN, I., CARMEL, L., WOLF, Y. I., MORI, H., SAVCHENKO, A. V., ARROWSMITH, C. H., KOONIN, E. V., EDWARDS, A. M. & YAKUNIN, A. F. 2006.

Genome-wide Analysis of Substrate Specificities of the Escherichia coli Haloacid Dehalogenase-like Phosphatase Family. *J Biol Chem,* 281**,** 36149-36161.

LAEMMLI, U. K. 1970. Cleavage of Structural Proteins during the Assembly of the Head of BActeriophage T4. *Nature,* 227**,** 680-685.

LEBLOND, D. J. & ROBINSON, J. L. 1976. Secondary Kinase Reactions Catalyzed by Yeast Pyruvate Kinase. *Biochim Biophys Acta,* 438**,** 108-113.

LINSTER, C. L., VAN SCHAFTINGEN, E. & HANSON, A. D. 2013. Metabolite damage and its repair or pre-emption. *Nat Chem Biol,* 9**,** 72-80.

LIPINSKI, C. A., LOMBARDO, F., DOMINY, B. W. & FEENEY, P. J. 1997. Experimental and computational approaches to estimate solubility and permeability in drug discovery and development settings. *Advanced Drug Delivery Reviews,* 23**,** 3-25.

LOPASCHUK, G. D., WALL, S. R., OLLEY, P. M. & DAVIES, N. J. 1988. Etomoxir, a Carnitine Palmitoyltransferase I Inhibitor, Protects Herats From Fatty Acid-Induced Ischemic Injury Independent of Changes in Long Chain Acycarnitine. *Circulation Research,* 63**,** 1036-1043.

LU, Z. & HUNTER, T. 2018. Metabolic Kinases Moonlighting as Protein Kinases. *Trends in Biochemical Sciences,* 43**,** 301-310.

MAYER, N., SCHWEIGER, M., ROMAUCH, M., GRABNER, G. F., EICHMANN, T. O., FUCHS, E., IVKOVIC, J., HEIER, C., MRAK, I., LASS, A., HOFLER, G., FLEDELIUS, C., ZECHNER, R., ZIMMERMANN, R. & BREINBAUER, R. 2013. Development of small-molecule inhibitors targeting adipose triglyceride lipase. *Nat Chem Biol,* 9**,** 785-7.

MORRISON, H., JERNSTRÖM, B., NORDENSKJÖLD, M., THOR, H. & ORRENIUS, S. 1984. Induction of DNA Damage by Menadione (2-Methyl-1,4-Naphthoquinone) in Primary Cultures of Rat Hepatocytes. *Biochemical Pharmacology,* 33**,** 1763-1769.

MUGABO, Y., ZHAO, S., SEIFRIED, A., GEZZAR, S., AL-MASS, A., ZHANG, D., LAMONTAGNE, J., ATTANE, C., POURSHARIFI, P., IGLESIAS, J., JOLY, E., PEYOT, M. L., GOHLA, A., MADIRAJU, S. R. & PRENTKI, M. 2016. Identification of a mammalian glycerol-3-phosphate phosphatase: Role in metabolism and signaling in pancreatic beta-cells and hepatocytes. *Proc Natl Acad Sci U S A,* 113**,** E430-9.

NEEDHAM, E. J., PARKER, B. L., BURYKIN, T., JAMES, D. E. & HUMPHREY, S. J. 2019. Illuminating the dark phosphoproteome. *Sci. Signal.,* 12**,** 1-18.

NEFF, C. D., ABKEVICH, V., PACKER, J. C., CHEN, Y., POTTER, J., RILEY, R., DAVENPORT, C., DEGRADO WARREN, J., JAMMULAPATI, S., BHATHENA, A., CHOI, W. S., KROEGER, P. E., METZGER, R. E., GUTIN, A., SKOLNICK, M. H., SHATTUCK, D. & KATZ, D. A. 2009. Evidence for HTR1A and LHPP as interacting genetic risk factors in major depression. *Mol Psychiatry,* 14**,** 621-30.

NYE, C., KIM, J., KALHAN, S. C. & HANSON, R. W. 2008. Reassessing triglyceride synthesis in adipose tissue. *Trends Endocrinol Metab,* 19**,** 356-61.

OLSEN, J. V., BLAGOEV, B., GNAD, F., MACEK, B., KUMAR, C., MORTENSEN, P. & MANN, M. 2006. Global, in vivo, and site-specific phosphorylation dynamics in signaling networks. *Cell,* 127**,** 635-48.

PARRINELLO, S., SAMPER, E., KRTOLICA, A., GOLDSTEIN, J., MELOV, S. & CAMPISI, J. 2003. Oxygen sensitivity limits the replicative lifespan of murine fibroblasts. *Nat Cell Biol,* 5**,** 741-747.

PARSONS, Z. D. & GATES, K. S. 2013. Thiol-dependent recovery of catalytic activity from oxidized protein tyrosine phosphatases. *Biochemistry,* 52**,** 6412-23.

PELLICER, M. T., NUÑEZ, M. F., AGUILAR, J., BADIA, J. & BALDOMA, L. 2003. Role of 2-Phosphoglycolate Phosphatase of Escherichia coli in Metabolism of the 2-Phosphoglycolate Formed in DNA Repair. *Journal of Bacteriology,* 185**,** 5815-5821.

PIERALISI, A., MARTINI, C., SOTO, D., VILA, M. C., CALVO, J. C. & GUERRA, L. N. 2016. N-acetylcysteine inhibits lipid accumulation in mouse embryonic adipocytes. *Redox Biol,* 9**,** 39-44.

PRENTKI, M. & MADIRAJU, S. R. 2008. Glycerolipid metabolism and signaling in health and disease. *Endocr Rev,* 29**,** 647-76.

RHEE, S. G., BAE, Y. S., LEE, S.-R. & KWON, J. 2000. Hydrogen Peroxide: A Key Messenger That Modulates Protein Phosphorylation Through Cysteine Oxidation. *Sci. STKE,* 53**,** 1-6.

RICHARDSON, K. E. & TOLBERT, N. E. 1961. Phosphoglycolic Acid Phosphatase. *J Biol Chem,* 236**,** 1285-1290.

ROSE, Z. B. & DUBE, S. 1978. Phosphoglycerate Mutase. *J Biol Chem,* 253**,** 8583-8592.

ROSE, Z. B. & LIEBOWITZ, J. 1970. 2,3-Diphosphoglycerate Phosphatase from Human Erythrocytes. General Properties and Activation by Anions. *J Biol Chem,* 245**,** 3232-3241.

SAMUNI, Y., GOLDSTEIN, S., DEAN, O. M. & BERK, M. 2013. The chemistry and biological activities of N-acetylcysteine. *Biochim Biophys Acta,* 1830**,** 4117-29.

SCHULZE, M., FEDORCHENKO, O., ZINK, T. G., KNOBBE-THOMSEN, C. B., KRAUS, S., SCHWINN, S., BEILHACK, A., REIFENBERGER, G., MONORANU, C. M., SIREN, A. L., JEANCLOS, E. & GOHLA, A. 2016. Chronophin is a glial tumor modifier involved in the regulation of glioblastoma growth and invasiveness. *Oncogene,* 35**,** 3163-77.

SEGERER, G. 2015. *Characterization of cell biological and physiological functions of the phosphoglycolate phosphatase AUM.* Doctor of Philosophy (Ph.D.) Doctoral dissertation, University of Würzburg, Germany.

SEGERER, G., ENGELMANN, D., KAESTNER, A., TROTZMULLER, M., KOFELER, H., STIGLOHER, C., THIELE, C., JEANCLOS, E. & GOHLA, A. 2018. A phosphoglycolate phosphatase/AUM-dependent link between triacylglycerol turnover and epidermal growth factor signaling. *Biochim Biophys Acta,* 1863**,** 584-594.

SEGERER, G., HADAMEK, K., ZUNDLER, M., FEKETE, A., SEIFRIED, A., MUELLER, M. J., KOENTGEN, F., GESSLER, M., JEANCLOS, E. & GOHLA, A. 2016. An essential developmental function for murine phosphoglycolate phosphatase in safeguarding cell proliferation. *Sci Rep,* 6**,** 35160.

SEIFRIED, A. 2014. *Mechanistic insights into specificity determinats and catalytic properties of the haloacid dehalogenase-type phosphatase AUM.* Doctor of Philosophy (Ph.D.) Doctoral dissertation, University of Würzburg, Germany.

SEIFRIED, A., BERGERON, A., BOIVIN, B. & GOHLA, A. 2016. Reversible oxidation controls the activity and oligomeric state of the mammalian phosphoglycolate phosphatase AUM. *Free Radic Biol Med,* 97**,** 75-84.

SEIFRIED, A., KNOBLOCH, G., DURAPHE, P. S., SEGERER, G., MANHARD, J., SCHINDELIN, H., SCHULTZ, J. & GOHLA, A. 2014. Evolutionary and structural analyses of

mammalian haloacid dehalogenase-type phosphatases AUM and chronophin provide insight into the basis of their different substrate specificities. *J Biol Chem,* 289**,** 3416-31.

SEIFRIED, A., SCHULTZ, J. & GOHLA, A. 2013. Human HAD phosphatases: structure, mechanism, and roles in health and disease. *FEBS J,* 280**,** 549-71.

SHARMA, R. 2012. *Enzyme Inhibition: Mechanisms and Scope, Enzyme Inhibition and Bioapplications*, InTech.

SIES, H., BERNDT, C. & JONES, D. P. 2017. Oxidative Stress. *Annu Rev Biochem,* 86**,** 715-748.

SILVERMAN, R. B. & HOLLADAY, M. W. 2014. *The Organic Chemistry of Drug Design and Drug Action,* San Diego, CA, Elsevier.

SMITH, P. K., KROHN, R. I., HERMANSON, G. T., MALLIA, A. K., GARTNER, F. H., PROVENZANO, M. D., FUJIMOTO, E. K., GOEKE, N. M., OLSON, B. J. & KLENK, D. C. 1985. Measurement of Protein Using Bicinchoninic Acid. *Anal Biochem,* 150**,** 76-85.

STIFFIN, R. M., SULLIVAN, S. M., CARLSON, G. M. & HOLYOAK, T. 2008. Differential Inhibition of Cytosolic PEPCK by Substrate Analogues. Kinetic and Structural Characterization of Inhibitor Recognition. *Biochemistry,* 47**,** 2099-2109.

STUBBE, J. & KOZARICH, J. W. 1987. Mechanisms of bleomycin-Induced DNA Degradation. *Chemical Reviews,* 87**,** 1107-1136.

SWINGLE, M., NI, L. & HONKANEN, R. E. 2007. Small-Molecule Inhibitors of Ser/Thr Protein Phosphatases: Specificity, Use and Common Forms of Abuse. *Methods Mol Biol.*

TAKAHASHI, T., TADA, M., IGARASHI, S., KOYAMA, A., DATE, H., YOKOSEKI, A., SHIGA, A., YOSHIDA, Y., TSUJI, S., NISHIZAWA, M. & ONODERA, O. 2007. Aprataxin, causative gene product for EAOH/AOA1, repairs DNA single-strand breaks with damaged 3'-phosphate and 3'-phosphoglycolate ends. *Nucleic Acids Res,* 35**,** 3797-809.

TREMBLAY, L. W., DUNAWAY-MARIANO, D. & ALLEN, K. N. 2006. Structure and Activity Analyses of Escheria coli K-12 NagD Provide Insight into the Evolution of Biochemical Function in the Haoalkanoic Acid Dehalogenase Superfamily. *Biochemistry,* 45**,** 1183-1193.

XIAO, H., WU, M., SHAO, F., GUAN, G., HUANG, B., TAN, B. & YIN, Y. 2016. N-Acetyl-L-cysteine Protects the Enterocyte against Oxidative Damage by Modulation of Mitochondrial Function. *Mediators Inflamm,* 2016**,** 8364279.

YEN, C. L., STONE, S. J., KOLIWAD, S., HARRIS, C. & FARESE, R. V., JR. 2008. Thematic review series: glycerolipids. DGAT enzymes and triacylglycerol biosynthesis. *J Lipid Res,* 49**,** 2283-301.

YI, D., HOU, Y., WANG, L., LONG, M., HU, S., MEI, H., YAN, L., HU, C. A. & WU, G. 2016. N-acetylcysteine stimulates protein synthesis in enterocytes independently of glutathione synthesis. *Amino Acids,* 48**,** 523-33.

ZENG, F. & HARRIS, R. C. 2014. Epidermal growth factor, from gene organization to bedside. *Semin Cell Dev Biol,* 28**,** 2-11.

7.2 Figures

7.3 Tables

7.4 Abbreviations

#1	inhibitor #1
#2	inhibitor #2
#9	inhibitor #9
#51	inhibitor #51
2PL	2-phospho-L-lactate
4PE	4-phospho-D-erythronate
× *g*	multiples of Earth's standard gravity (9.81m·s-2)
µg	microgram
µL	microliter
ADP	adenosine diphosphate
APE1	apurinic/apyrimidinic endonuclease 1
Asp	aspartate
ATP	adenosine triphosphate
AUM	aspartate-based ubiquitous Mg^{2+}-dependent phosphatase, cf. PGP
BLM	bleomycin
BPG	bisphosphoglycerate
C	cysteine
CIN	Chronophin, cf. PDXP
cm	centimeter
Cys	cysteine
D	aspartate
Da	Dalton
DGAT	diglyceride acyltransferase
DiFMUP	6,8-difluoro-4-methylumbelliferyl phosphate
DNA	deoxyribonucleic acid
dNTP	deoxyribonucleotide
E	glutamic acid
EDTA	ethylenediaminetetraacetic acid
EGF	epidermal growth factor

EGFR	epidermal growth factor receptor
EI	enzyme-inhibitor complex
EIS	enzyme-inhibitor-substrate-complex
EP	enzyme-product-complex
ES	enzyme-substrate-complex
ESI	enzyme-substrate-inhibitor-complex
G	glycine
g/mol	molar mass
GC1	murine spermatogonial cell line
GDP	guanosine diphosphate
Gro3P	glycerol-3-phosphate
GTP	guanosine triphosphate
h	hydrophobic amino acid
H	histidine
H_2O	molecular water
H_2O_2	hydrogen peroxide
HAD	haloacid dehalogenase
His	histidine
kb	kilobases
kDa	kilo Dalton
K_i	inhibitor dissociation constant
K_M	Michaelis-Menten-constant
L	leucin
LDH	lactate dehydrogenase
Leu	leucin
min	minute
mL	milliliter
mM	millimolar
MN	menadione
n. t.	no treatment

NAC	N-acetylcysteine
ng	nanogram
nm	nanometer
nM	nanomolar
O_2	molecular oxygen
PDXP	pyridoxal phosphatase
PG	phosphoglycolate
PGP	phosphoglycolate phosphatase
PLP	pyridoxal 5'-phosphate
pNPP	para-nitrophenyl phosphate
PSTP	protein serine/threonine phosphatase
PTP	protein tyrosine phosphatase
RNA	ribonucleic acid
rpm	rotations per minute
S	serine
SEM	standard error of the mean
Ser	serine
shRNA	small hairpin RNA
siRNA	small interfering RNA
T	threonine
TDP1	tyrosyl-DNA phosphodiesterase 1
Thr	threonine
V	valine
v/v	volume/volume
v_{max}	maximum velocity of enzymatic catalysis
w/v	weight/volume
WT	wildtype
x	any amino acid

Publications and Conference Contributions

Research articles

SEGERER, G., ENGELMANN, D., KAESTNER, A., TROTZMULLER, M., KOFELER, H., STIGLOHER, C., THIELE, C., JEANCLOS, E. & GOHLA, A. 2018. A phosphoglycolate phosphatase/AUM-dependent link between triacylglycerol turnover and epidermal growth factor signaling. *Biochim Biophys Acta,* 1863**,** 584-594.

Oral Presentations

March 2017 Interdisciplinary seminar for medical doctorands: "Functional characterization of the Phosphoglycolate Phosphatase AUM: role in cell proliferation and characterization of small molecule inhibitors"

Nov. 2017 Interdisciplinary seminar for medical doctorands: "Biochemical characterization of Phosphoglycolate Phosphatase inhibitors"

Poster Presentations

June 2017 10th GSLS Retreat: "Biochemical characterization of Phosphoglycolate Phosphatase inhibitors"

Oct. 2017 12th International GSLS Student Symposium: "Biochemical characterization of Phosphoglycolate Phosphatase inhibitors"

Affidavit

I hereby confirm that my thesis entitled "Regulation of Mammalian Phosphoglycolate Phosphatase " is the result of my own work. I did not receive any help or support from commercial consultants. All sources and/or materials applied are listed and specified in the thesis.

Furthermore, I confirm that this thesis has not yet been submitted as part of another examination process neither in identical nor similar form.

Würzburg _____

Date Signature

Acknowledgements

First and foremost, I would like to thank the Gohla group for its extraordinary support with my doctoral thesis. My supervisor Prof. Dr. Antje Gohla has always taken the necessary time to discuss my project and the results. Dr. Gabriela Segerer, Dr. Elisabeth Jeanclos, Stefanie Hüttl, Kerstin Hadamek, and Angelika Keller have taught me important skills for the laboratory work and have always had a sympathetic ear for questions.

The GSLS and its employees deserve a big thank you, as the structured MD program facilitates the introduction into scientific work. I thank my co-supervisors Prof. Dr. Stefan Gaubatz and Prof. Dr. Andreas Geier for their interest in my work.

And of course, I would like to thank Leo and my family for unconditional support of any kind.